Review | Vol. 8, No. 3 | 1 Mar 2017 | BIOMEDICAL OPTICS EXPRESS 1607

Biomedical Optics EXPRESS

Review of intraoperative optical coherence tomography: technology and applications [Invited]

Oscar M. Carrasco-Zevallos,[1,*] Christian Viehland,[1] Brenton Keller,[1] Mark Draelos,[1] Anthony N. Kuo,[2] Cynthia A. Toth,[1,2] and Joseph A. Izatt[1,2]

[1]*Department of Biomedical Engineering, Duke University, Durham, NC 27708, USA*
[2]*Department of Ophthalmology, Duke University Medical Center, NC 27710, USA*
[*]*omc3@duke.edu*

Abstract: During microsurgery, *en face* imaging of the surgical field through the operating microscope limits the surgeon's depth perception and visualization of instruments and sub-surface anatomy. Surgical procedures outside microsurgery, such as breast tumor resections, may also benefit from visualization of the sub-surface tissue structures. The widespread clinical adoption of optical coherence tomography (OCT) in ophthalmology and its growing prominence in other fields, such as cancer imaging, has motivated the development of intraoperative OCT for real-time tomographic visualization of surgical interventions. This article reviews key technological developments in intraoperative OCT and their applications in human surgery. We focus on handheld OCT probes, microscope-integrated OCT systems, and OCT-guided laser treatment platforms designed for intraoperative use. Moreover, we discuss intraoperative OCT adjuncts and processing techniques currently under development to optimize the surgical feedback derivable from OCT data. Lastly, we survey salient clinical studies of intraoperative OCT for human surgery.

OCIS codes: (110.4500) Optical coherence tomography; (170.0110) Imaging systems.

References and links

1. R. K. Daniel, "Microsurgery: through the looking glass," N. Engl. J. Med. **300**(22), 1251–1257 (1979).
2. M. Singh and A. Saxena, "Microsurgery: A Useful and Versatile Tool in Surgical Field," Surg. Curr. Res. **4**(4), 9–11 (2014).
3. J. M. Parel, R. Machemer, and W. Aumayr, "A new concept for vitreous surgery. 5. An automated operating microscope," Am. J. Ophthalmol. **77**(2), 161–168 (1974).
4. R. Machemer, H. Buettner, E. W. Norton, and J. M. Parel, "Vitrectomy: a pars plana approach," Trans. Am. Acad. Ophthalmol. Otolaryngol. **75**(4), 813–820 (1971).
5. M. Hubschmann and W. Bauersfeld, "Instrument for rapid examination of transparent microscopic preparations," US Patent 1943508 A, 1931.
6. B. Todorich, C. Shieh, P. J. DeSouza, O. M. Carrasco-Zevallos, D. L. Cunefare, S. S. Stinnett, J. A. Izatt, S. Farsiu, P. Mruthyunjaya, A. N. Kuo, and C. A. Toth, "Impact of microscope integrated OCT on ophthlamology resident performance of anterior segment surgical manuevers in model eyes," Invest. Ophthalmol. Vis. Sci. **57**(9), OCT146 (2016).
7. A. W. Scott, S. Farsiu, L. B. Enyedi, D. K. Wallace, and C. A. Toth, "Imaging the infant retina with a hand-held spectral-domain optical coherence tomography device," Am. J. Ophthalmol. **147**(2), 364–373 (2009).
8. G. E. Keles, K. R. Lamborn, and M. S. Berger, "Low-grade hemispheric gliomas in adults: a critical review of extent of resection as a factor influencing outcome," J. Neurosurg. **95**(5), 735–745 (2001).
9. M. Lacroix, D. Abi-Said, D. R. Fourney, Z. L. Gokaslan, W. Shi, F. DeMonte, F. F. Lang, I. E. McCutcheon, S. J. Hassenbusch, E. Holland, K. Hess, C. Michael, D. Miller, and R. Sawaya, "A multivariate analysis of 416 patients with glioblastoma multiforme: prognosis, extent of resection, and survival," J. Neurosurg. **95**(2), 190–198 (2001).
10. S. J. Schnitt, A. Abner, R. Gelman, J. L. Connolly, A. Recht, R. B. Duda, T. J. Eberlein, K. Mayzel, B. Silver, and J. R. Harris, "The relationship between microscopic margins of resection and the risk of local recurrence in patients with breast cancer treated with breast-conserving surgery and radiation therapy," Cancer **74**(6), 1746–1751 (1994).

#281779 https://doi.org/10.1364/BOE.8.001607
Journal © 2017 Received 30 Nov 2016; revised 9 Feb 2017; accepted 9 Feb 2017; published 21 Feb 2017

Biomedical Optics EXPRESS

11. R. Holland, S. H. Veling, M. Mravunac, and J. H. Hendriks, "Histologic multifocality of Tis, T1-2 breast carcinomas. Implications for clinical trials of breast-conserving surgery," Cancer **56**(5), 979–990 (1985).
12. S. F. Berkovic, A. M. McIntosh, R. M. Kalnins, G. D. Jackson, G. C. Fabinyi, G. A. Brazenor, P. F. Bladin, and J. L. Hopper, "Preoperative MRI predicts outcome of temporal lobectomy: an actuarial analysis," Neurology **45**(7), 1358–1363 (1995).
13. C. R. Rossi, S. Mocellin, B. Scagnet, M. Foletto, A. Vecchiato, P. Pilati, A. Tregnaghi, G. Zavagno, R. Stramare, L. Rubaltelli, C. Montesco, S. Borsato, D. Rubello, and M. Lise, "The role of preoperative ultrasound scan in detecting lymph node metastasis before sentinel node biopsy in melanoma patients," J. Surg. Oncol. **83**(2), 80–84 (2003).
14. D. Goutallier, J. M. Postel, J. Bernageau, L. Lavau, and M. C. Voisin, "Fatty Muscle Degeneration in Cuff Ruptures. Pre- and Postoperative Evaluation by CT Scan," Clin. Orthop. Relat. Res. **304**, 78–83 (1994).
15. R. M. Comeau, A. F. Sadikot, A. Fenster, and T. M. Peters, "Intraoperative ultrasound for guidance and tissue shift correction in image-guided neurosurgery," Med. Phys. **27**(4), 787–800 (2000).
16. H. Neshat, D. W. Cool, K. Barker, L. Gardi, N. Kakani, and A. Fenster, "A 3D ultrasound scanning system for image guided liver interventions," Med. Phys. **40**(11), 112903 (2013).
17. H. G. Kenngott, M. Wagner, M. Gondan, F. Nickel, M. Nolden, A. Fetzer, J. Weitz, L. Fischer, S. Speidel, H.-P. Meinzer, D. Böckler, M. W. Büchler, and B. P. Müller-Stich, "Real-time image guidance in laparoscopic liver surgery: first clinical experience with a guidance system based on intraoperative CT imaging," Surg. Endosc. **28**(3), 933–940 (2014).
18. D. J. Brenner and E. J. Hall, "Computed tomography--an increasing source of radiation exposure," N. Engl. J. Med. **357**(22), 2277–2284 (2007).
19. V. M. Tronnier, C. R. Wirtz, M. Knauth, G. Lenz, O. Pastyr, M. M. Bonsanto, F. K. Albert, R. Kuth, A. Staubert, W. Schlegel, K. Sartor, and S. Kunze, "Intraoperative diagnostic and interventional magnetic resonance imaging in neurosurgery," Neurosurgery **40**(5), 891–902 (1997).
20. C. Senft, A. Bink, K. Franz, H. Vatter, T. Gasser, and V. Seifert, "Intraoperative MRI guidance and extent of resection in glioma surgery: a randomised, controlled trial," Lancet Oncol. **12**(11), 997–1003 (2011).
21. G. M. van Dam, G. Themelis, L. M. Crane, N. J. Harlaar, R. G. Pleijhuis, W. Kelder, A. Sarantopoulos, J. S. de Jong, H. J. Arts, A. G. van der Zee, J. Bart, P. S. Low, and V. Ntziachristos, "Intraoperative tumor-specific fluorescence imaging in ovarian cancer by folate receptor-α targeting: first in-human results," Nat. Med. **17**(10), 1315–1319 (2011).
22. A. L. Vahrmeijer, M. Hutteman, J. R. van der Vorst, C. J. H. van de Velde, and J. V. Frangioni, "Image-guided cancer surgery using near-infrared fluorescence," Nat. Rev. Clin. Oncol. **10**(9), 507–518 (2013).
23. E. M. Sevick-Muraca, W. J. Akers, B. P. Joshi, G. D. Luker, C. S. Cutler, L. J. Marnett, C. H. Contag, T. D. Wang, and A. Azhdarinia, "Advancing the translation of optical imaging agents for clinical imaging," Biomed. Opt. Express **4**(1), 160–170 (2013).
24. D. Huang, E. A. Swanson, C. P. Lin, J. S. Schuman, W. G. Stinson, W. Chang, M. R. Hee, T. Flotte, K. Gregory, C. A. Puliafito, and J. G. Fujimoto, "Optical coherence tomography," Science **254**(5035), 1178–1181 (1991).
25. F. Fercher, K. Hitzenberger, G. Kamp, and S. Y. El-Zaiat, "Measurement of intraocular distances by backscattering spectral interferometry," Opt. Commun. **117**(1-2), 43–48 (1995).
26. G. Hä Usler and M. W. Lindner, "'Coherence Radar' and 'Spectral Radar'-New Tools for Dermatological Diagnosis," J. Biomed. Opt. **3**(1), 21–31 (1998).
27. S. R. Chinn, E. A. Swanson, and J. G. Fujimoto, "Optical coherence tomography using a frequency-tunable optical source," Opt. Lett. **22**(5), 340–342 (1997).
28. B. Golubovic, B. E. Bouma, G. J. Tearney, and J. G. Fujimoto, "Optical frequency-domain reflectometry using rapid wavelength tuning of a Cr4+:forsterite laser," Opt. Lett. **22**(22), 1704–1706 (1997).
29. R. Leitgeb, C. Hitzenberger, and A. Fercher, "Performance of fourier domain vs. time domain optical coherence tomography," Opt. Express **11**(8), 889–894 (2003).
30. J. F. de Boer, B. Cense, B. H. Park, M. C. Pierce, G. J. Tearney, and B. E. Bouma, "Improved signal-to-noise ratio in spectral-domain compared with time-domain optical coherence tomography," Opt. Lett. **28**(21), 2067–2069 (2003).
31. M. Choma, M. Sarunic, C. Yang, and J. Izatt, "Sensitivity advantage of swept source and Fourier domain optical coherence tomography," Opt. Express **11**(18), 2183–2189 (2003).
32. A. Rollins, S. Yazdanfar, M. Kulkarni, R. Ung-Arunyawee, and J. Izatt, "In vivo video rate optical coherence tomography," Opt. Express **3**(6), 219–229 (1998).
33. N. Nassif, B. Cense, B. Park, M. Pierce, S. Yun, B. Bouma, G. Tearney, T. Chen, and J. de Boer, "In vivo high-resolution video-rate spectral-domain optical coherence tomography of the human retina and optic nerve," Opt. Express **12**(3), 367–376 (2004).
34. W. Wieser, W. Draxinger, T. Klein, S. Karpf, T. Pfeiffer, and R. Huber, "High definition live 3D-OCT in vivo: design and evaluation of a 4D OCT engine with 1 GVoxel/s," Biomed. Opt. Express **5**(9), 2963–2977 (2014).
35. K. Zhang and J. U. Kang, "Real-time 4D signal processing and visualization using graphics processing unit on a regular nonlinear-k Fourier-domain OCT system," Opt. Express **18**(11), 11772–11784 (2010).
36. D. H. Choi, H. Hiro-Oka, K. Shimizu, and K. Ohbayashi, "Spectral domain optical coherence tomography of multi-MHz A-scan rates at 1310 nm range and real-time 4D-display up to 41 volumes/second," Biomed. Opt. Express **3**(12), 3067–3086 (2012).

Biomedical Optics EXPRESS

37. J. G. Fujimoto, C. Pitris, S. A. Boppart, and M. E. Brezinski, "Optical Coherence Tomography: An Emerging Technology for Biomedical Imaging and Optical Biopsy," Neoplasia **2**(1-2), 9–25 (2000).
38. C. A. Toth, D. G. Narayan, S. A. Boppart, M. R. Hee, J. G. Fujimoto, R. Birngruber, C. P. Cain, C. D. DiCarlo, and W. P. Roach, "A Comparison of Retinal Morphology Viewed by Optical Coherence Tomography and by Light Microscopy," Arch. Ophthalmol. **115**(11), 1425–1428 (1997).
39. B. Potsaid, B. Baumann, D. Huang, S. Barry, A. E. Cable, J. S. Schuman, J. S. Duker, and J. G. Fujimoto, "Ultrahigh speed 1050nm swept source/Fourier domain OCT retinal and anterior segment imaging at 100,000 to 400,000 axial scans per second," Opt. Express **18**(19), 20029–20048 (2010).
40. B. Cense, N. Nassif, T. Chen, M. Pierce, S. H. Yun, B. Park, B. Bouma, G. Tearney, and J. de Boer, "Ultrahigh-Resolution High-Speed Retinal Imaging Using Spectral-Domain Optical Coherence Tomography," Opt. Express **12**(11), 2435–2447 (2004).
41. M. Wojtkowski, R. Leitgeb, A. Kowalczyk, T. Bajraszewski, and A. F. Fercher, "In vivo human retinal imaging by Fourier domain optical coherence tomography," J. Biomed. Opt. **7**(3), 457–463 (2002).
42. J. Fujimoto and E. Swanson, "The development, commercialization, and impact of optical coherence tomography," Invest. Ophthalmol. Vis. Sci. **57**(9), OCT1–OCT13 (2016).
43. E. A. Swanson, J. A. Izatt, M. R. Hee, D. Huang, C. P. Lin, J. S. Schuman, C. A. Puliafito, and J. G. Fujimoto, "In vivo retinal imaging by optical coherence tomography," Opt. Lett. **18**(21), 1864–1866 (1993).
44. J. A. Izatt, M. R. Hee, E. A. Swanson, C. P. Lin, D. Huang, J. S. Schuman, C. A. Puliafito, and J. G. Fujimoto, "Micrometer-Scale Resolution Imaging of the Anterior Eye in Vivo with Optical Coherence Tomography," Arch. Ophthalmol. **112**(12), 1584–1589 (1994).
45. J. S. Schuman, C. A. Puliafito, J. G. Fujimoto, and J. S. Duker, *Optical Coherence Tomography of Ocular Diseases*, 3rd ed. SLACK Incorporated, 2013.
46. H. Yoo, J. W. Kim, M. Shishkov, E. Namati, T. Morse, R. Shubochkin, J. R. McCarthy, V. Ntziachristos, B. E. Bouma, F. A. Jaffer, and G. J. Tearney, "Intra-arterial catheter for simultaneous microstructural and molecular imaging in vivo," Nat. Med. **17**(12), 1680–1684 (2011).
47. M. J. Gora, J. S. Sauk, R. W. Carruth, K. A. Gallagher, M. J. Suter, N. S. Nishioka, L. E. Kava, M. Rosenberg, B. E. Bouma, and G. J. Tearney, "Tethered capsule endomicroscopy enables less invasive imaging of gastrointestinal tract microstructure," Nat. Med. **19**(2), 238–240 (2013).
48. S. A. Boppart, W. Luo, D. L. Marks, and K. W. Singletary, "Optical coherence tomography: feasibility for basic research and image-guided surgery of breast cancer," Breast Cancer Res. Treat. **84**(2), 85–97 (2004).
49. B. J. Vakoc, D. Fukumura, R. K. Jain, and B. E. Bouma, "Cancer imaging by optical coherence tomography: preclinical progress and clinical potential," Nat. Rev. Cancer **12**(5), 363–368 (2012).
50. O. Assayag, K. Grieve, B. Devaux, F. Harms, J. Pallud, F. Chretien, C. Boccara, and P. Varlet, "Imaging of non-tumorous and tumorous human brain tissues with full-field optical coherence tomography," Neuroimage Clin. **2**(1), 549–557 (2013).
51. B. J. Vakoc, R. M. Lanning, J. A. Tyrrell, T. P. Padera, L. A. Bartlett, T. Stylianopoulos, L. L. Munn, G. J. Tearney, D. Fukumura, R. K. Jain, and B. E. Bouma, "Three-dimensional microscopy of the tumor microenvironment in vivo using optical frequency domain imaging," Nat. Med. **15**(10), 1219–1223 (2009).
52. J. R. Wilkins, C. A. Puliafito, M. R. Hee, J. S. Duker, E. Reichel, J. G. Coker, J. S. Schuman, E. A. Swanson, and J. G. Fujimoto, "Characterization of epiretinal membranes using optical coherence tomography," Ophthalmology **103**(12), 2142–2151 (1996).
53. C. A. Toth, R. Birngruber, S. A. Boppart, M. R. Hee, J. G. Fujimoto, C. D. DiCarlo, E. A. Swanson, C. P. Cain, D. G. Narayan, G. D. Noojin, and W. P. Roach, "Argon laser retinal lesions evaluated in vivo by optical coherence tomography," Am. J. Ophthalmol. **123**(2), 188–198 (1997).
54. G. Ripandelli, A. M. Coppé, S. Bonini, R. Giannini, S. Curci, E. Costi, and M. Stirpe, "Morphological evaluation of full-thickness idiopathic macular holes by optical coherence tomography," Eur. J. Ophthalmol. **9**(3), 212–216 (1999).
55. K. Mikajiri, A. A. Okada, M. Ohji, T. Morimoto, S. Sato, A. Hayashi, S. Kusaka, Y. Saito, and Y. Tano, "Analysis of vitrectomy for idiopathic macular hole by optical coherence tomography," Am. J. Ophthalmol. **128**(5), 655–657 (1999).
56. R. P. Gallemore, J. M. Jumper, B. W. McCuen 2nd, G. J. Jaffe, E. A. Postel, and C. A. Toth, "Diagnosis of vitreoretinal adhesions in macular disease with optical coherence tomography," Retina **20**(2), 115–120 (2000).
57. P. Massin, C. Allouch, B. Haouchine, F. Metge, M. Paques, L. Tangui, A. Erginay, and A. Gaudric, "Optical coherence tomography of idiopathic macular epiretinal membranes before and after surgery," Am. J. Ophthalmol. **130**(6), 732–739 (2000).
58. C. I. Falkner-Radler, C. Glittenberg, S. Hagen, T. Benesch, and S. Binder, "Spectral-domain optical coherence tomography for monitoring epiretinal membrane surgery," Ophthalmology **117**(4), 798–805 (2010).
59. J. M. Jumper, R. P. Gallemore, B. W. McCuen 2nd, and C. A. Toth, "Features of Macular Hole Closure in the Early Postoperative Period Using Optical Coherence Tomography," Retina **20**(3), 232–237 (2000).
60. Y. Kasuga, J. Arai, M. Akimoto, and N. Yoshimura, "Optical coherence tomograghy to confirm early closure of macular holes," Am. J. Ophthalmol. **130**(5), 675–676 (2000).
61. J. Akiba, S. Konno, E. Sato, and A. Yoshida, "Retinal detachment and retinoschisis detected by optical coherence tomography in a myopic eye with a macular hole," Ophthalmic Surg. Lasers **31**(3), 240–242 (2000).
62. K. Kumagai, M. Furukawa, N. Ogino, and E. Larson, "Factors correlated with postoperative visual acuity after vitrectomy and internal limiting membrane peeling for myopic foveoschisis," Retina **30**(6), 874–880 (2010).

Biomedical Optics EXPRESS

63. A. Behrens, W. J. Stark, K. A. Pratzer, and P. J. McDonnell, "Dynamics of small-incision clear cornea wounds after phacoemulsification surgery using optical coherence tomography in the early postoperative period," J. Refract. Surg. **24**(1), 46–49 (2008).
64. R. P. McNabb, S. Farsiu, S. S. Stinnett, J. A. Izatt, and A. N. Kuo, "Optical coherence tomography accurately measures corneal power change from laser refractive surgery," Ophthalmology **122**(4), 677–686 (2015).
65. M. E. Brezinski, G. J. Tearney, S. A. Boppart, E. A. Swanson, J. F. Southern, and J. G. Fujimoto, "Optical biopsy with optical coherence tomography: feasibility for surgical diagnostics," J. Surg. Res. **71**(1), 32–40 (1997).
66. S. A. Boppart, B. E. Bouma, C. Pitris, G. J. Tearney, J. G. Fujimoto, and M. E. Brezinski, "Forward-imaging instruments for optical coherence tomography," Opt. Lett. **22**(21), 1618–1620 (1997).
67. S. Radhakrishnan, A. M. Rollins, J. E. Roth, S. Yazdanfar, V. Westphal, D. S. Bardenstein, and J. A. Izatt, "Real-time optical coherence tomography of the anterior segment at 1310 nm," Arch. Ophthalmol. **119**(8), 1179–1185 (2001).
68. J. Wei and T. Hellmuth, "Optical coherence tomography assisted ophthalmologic surgical microscope," US Patent 5493109 A, 1994.
69. S. A. Boppart, B. E. Bouma, C. Pitris, G. J. Tearney, J. F. Southern, M. E. Brezinski, and J. G. Fujimoto, "Intraoperative assessment of microsurgery with three-dimensional optical coherence tomography," Radiology **208**(1), 81–86 (1998).
70. E. Lankenau, D. Klinger, C. Winter, A. Malik, H. H. Müller, S. Oelckers, H.-W. Pau, T. Just, and G. Hüttmann, "Combining Optical Coherence Tomography (OCT) with an Operating Microscope," in *Advances in Medical Engineering*, 2007, pp. 343–348.
71. Y. K. Tao, J. P. Ehlers, C. A. Toth, and J. A. Izatt, "Intraoperative spectral domain optical coherence tomography for vitreoretinal surgery," Opt. Lett. **35**(20), 3315–3317 (2010).
72. S. A. Boppart, J. Herrmann, C. Pitris, D. L. Stamper, M. E. Brezinski, and J. G. Fujimoto, "High-resolution optical coherence tomography-guided laser ablation of surgical tissue," J. Surg. Res. **82**(2), 275–284 (1999).
73. D. V. Palanker, M. S. Blumenkranz, D. Andersen, M. Wiltberger, G. Marcellino, P. Gooding, D. Angeley, G. Schuele, B. Woodley, M. Simoneau, N. J. Friedman, B. Seibel, J. Batlle, R. Feliz, J. Talamo, and W. Culbertson, "Femtosecond laser-assisted cataract surgery with integrated optical coherence tomography," Sci. Transl. Med. **2**(58), 58ra85 (2010).
74. J. T. W. Yeow, V. X. D. Yang, A. Chahwan, M. L. Gordon, B. Qi, I. A. Vitkin, B. C. Wilson, and A. A. Goldenberg, "Micromachined 2-D scanner for 3-D optical coherence tomography," Sens. Actuators A Phys. **117**(2), 331–340 (2005).
75. W. Jung, J. Zhang, L. Wang, P. Wilder-Smith, Z. Chen, D. T. McCormick, and N. C. Tien, "Three-dimensional optical coherence tomography employing a 2-Axis MEMS," IEEE J. Sel. Top. Quantum Electron. **11**(4), 806–810 (2005).
76. C. D. Lu, M. F. Kraus, B. Potsaid, J. J. Liu, W. Choi, V. Jayaraman, A. E. Cable, J. Hornegger, J. S. Duker, and J. G. Fujimoto, "Handheld ultrahigh speed swept source optical coherence tomography instrument using a MEMS scanning mirror," Biomed. Opt. Express **5**(1), 293–311 (2014).
77. R. L. Shelton, W. Jung, S. I. Sayegh, D. T. McCormick, J. Kim, and S. A. Boppart, "Optical coherence tomography for advanced screening in the primary care office," J. Biophotonics **7**(7), 525–533 (2014).
78. F. LaRocca, D. Nankivil, T. DuBose, C. A. Toth, S. Farsiu, and J. A. Izatt, "In vivo cellular-resolution retinal imaging in infants and children using an ultracompact handheld probe," Nat. Photonics **10**(September), S80–S84 (2016).
79. W. Brown, E. Buckland, and J. A. Izatt, "Portable Optical Coherence Tomography (OCT) Devices and Related Systems," US Patent 20070081166A1, 2006.
80. P. N. Dayani, R. Maldonado, S. Farsiu, and C. A. Toth, "Intraoperative use of Handheld Spectral Domain Optical Coherence Tomography Imaging in Macular Surgery," Retina **29**(10), 1457–1468 (2009).
81. R. Ray, D. E. Barañano, J. A. Fortun, B. J. Schwent, B. E. Cribbs, C. S. Bergstrom, G. B. Hubbard 3rd, and S. K. Srivastava, "Intraoperative microscope-mounted spectral domain optical coherence tomography for evaluation of retinal anatomy during macular surgery," Ophthalmology **118**(11), 2212–2217 (2011).
82. J. P. Ehlers, W. J. Dupps, P. K. Kaiser, J. Goshe, R. P. Singh, D. Petkovsek, and S. K. Srivastava, "The Prospective Intraoperative and Perioperative Ophthalmic ImagiNg with Optical CoherEncE TomogRaphy (PIONEER) Study: 2-year results," Am. J. Ophthalmol. **158**(5), 999–1007 (2014).
83. S. H. Chavala, S. Farsiu, R. Maldonado, D. K. Wallace, S. F. Freedman, and C. A. Toth, "Insights into advanced retinopathy of prematurity using handheld spectral domain optical coherence tomography imaging," Ophthalmology **116**(12), 2448–2456 (2009).
84. R. S. Maldonado, R. V. O'Connell, N. Sarin, S. F. Freedman, D. K. Wallace, C. M. Cotten, K. P. Winter, S. Stinnett, S. J. Chiu, J. A. Izatt, S. Farsiu, and C. A. Toth, "Dynamics of human foveal development after premature birth," Ophthalmology **118**(12), 2315–2325 (2011).
85. R. S. Maldonado, J. A. Izatt, N. Sarin, D. K. Wallace, S. Freedman, C. M. Cotten, and C. A. Toth, "Optimizing hand-held spectral domain optical coherence tomography imaging for neonates, infants, and children," Invest. Ophthalmol. Vis. Sci. **51**(5), 2678–2685 (2010).
86. A. L. Rothman, F. A. Folgar, A. Y. Tong, and C. A. Toth, "Spectral domain optical coherence tomography characterization of pediatric epiretinal membranes," Retina **34**(7), 1323–1334 (2014).

Biomedical Optics EXPRESS

87. F. Pichi, M. Alkabes, P. Nucci, and A. P. Ciardella, "Intraoperative SD-OCT in macular surgery," Ophthalmic Surg. Lasers Imaging **43**(6 Suppl), S54–S60 (2012).
88. M. Riazi-Esfahani, M. R. Khademi, M. Mazloumi, A. Khodabandeh, and H. Riazi-Esfahani, "Macular surgery using intraoperative spectral domain optical coherence tomography," J. Ophthalmic Vis. Res. **10**(3), 309–315 (2015).
89. L. A. Branchini, K. Gurley, J. S. Duker, and E. Reichel, "Use of Handheld Intraoperative Spectral-Domain Optical Coherence Tomography in a Variety of Vitreoretinal Diseases," Ophthalmic Surg. Lasers Imaging Retina **47**(1), 49–54 (2016).
90. X. Li, S. Martin, C. Pitris, R. Ghanta, D. L. Stamper, M. Harman, J. G. Fujimoto, and M. E. Brezinski, "High-resolution optical coherence tomographic imaging of osteoarthritic cartilage during open knee surgery," Arthritis Res. Ther. **7**(2), R318–R323 (2005).
91. Y. Huang, G. J. Furtmüller, D. Tong, S. Zhu, W. P. A. Lee, G. Brandacher, and J. U. Kang, "MEMS-based handheld fourier domain Doppler optical coherence tomography for intraoperative microvascular anastomosis imaging," PLoS One **9**(12), e114215 (2014).
92. A. D. Aguirre, P. R. Hertz, Y. Chen, J. G. Fujimoto, W. Piyawattanametha, L. Fan, and M. C. Wu, "Two-axis MEMS scanning catheter for ultrahigh resolution three-dimensional and en face imaging," Opt. Express **15**(5), 2445–2453 (2007).
93. K. H. Kim, B. H. Park, G. N. Maguluri, T. W. Lee, F. J. Rogomentich, M. G. Bancu, B. E. Bouma, J. F. de Boer, and J. J. Bernstein, "Two-axis magnetically-driven MEMS scanning catheter for endoscopic high-speed optical coherence tomography," Opt. Express **15**(26), 18130–18140 (2007).
94. S. J. Erickson-Bhatt, R. M. Nolan, N. D. Shemonski, S. G. Adie, J. Putney, D. Darga, D. T. McCormick, A. J. Cittadine, A. M. Zysk, M. Marjanovic, E. J. Chaney, G. L. Monroy, F. A. South, K. A. Cradock, Z. G. Liu, M. Sundaram, P. S. Ray, and S. A. Boppart, "Real-time Imaging of the Resection Bed Using a Handheld Probe to Reduce Incidence of Microscopic Positive Margins in Cancer Surgery," Cancer Res. **75**(18), 3706–3712 (2015).
95. A. M. Zysk, K. Chen, E. Gabrielson, L. Tafra, E. A. May Gonzalez, J. K. Canner, E. B. Schneider, A. J. Cittadine, P. Scott Carney, S. A. Boppart, K. Tsuchiya, K. Sawyer, and L. K. Jacobs, "Intraoperative Assessment of Final Margins with a Handheld Optical Imaging Probe During Breast-Conserving Surgery May Reduce the Reoperation Rate: Results of a Multicenter Study," Ann. Surg. Oncol. **22**(10), 3356–3362 (2015).
96. F. Benboujja, J. A. Garcia, K. Beaudette, M. Strupler, C. J. Hartnick, and C. Boudoux, "Intraoperative imaging of pediatric vocal fold lesions using optical coherence tomography," J. Biomed. Opt. **21**(1), 016007 (2016).
97. S. A. Boppart, G. J. Tearney, B. E. Bouma, M. E. Brezinski, J. G. Fujimoto, and E. A. Swanson, "Methods and apparatus for forward-directed optical scanning instruments," US Patent 6485413B1, 1998.
98. X. Li, C. Chudoba, T. Ko, C. Pitris, and J. G. Fujimoto, "Imaging needle for optical coherence tomography," Opt. Lett. **25**(20), 1520–1522 (2000).
99. C.-P. Liang, J. Wierwille, T. Moreira, G. Schwartzbauer, M. S. Jafri, C.-M. Tang, and Y. Chen, "A forward-imaging needle-type OCT probe for image guided stereotactic procedures," Opt. Express **19**(27), 26283–26294 (2011).
100. C. Sun, K. K. C. Lee, B. Vuong, M. D. Cusimano, A. Brukson, A. Mauro, N. Munce, B. K. Courtney, B. A. Standish, and V. X. D. Yang, "Intraoperative handheld optical coherence tomography forward-viewing probe: physical performance and preliminary animal imaging," Biomed. Opt. Express **3**(6), 1404–1412 (2012).
101. A. M. Zysk, F. T. Nguyen, E. J. Chaney, J. G. Kotynek, U. J. Oliphant, F. J. Bellafiore, P. A. Johnson, K. M. Rowland, and S. A. Boppart, "Clinical feasibility of microscopically-guided breast needle biopsy using a fiber-optic probe with computer-aided detection," Technol. Cancer Res. Treat. **8**(5), 315–321 (2009).
102. N. V. Iftimia, M. Mujat, T. Ustun, R. D. Ferguson, V. Danthu, and D. X. Hammer, "Spectral-domain low coherence interferometry/optical coherence tomography system for fine needle breast biopsy guidance," Rev. Sci. Instrum. **80**(2), 024302 (2009).
103. R. A. McLaughlin, B. C. Quirk, A. Curatolo, R. W. Kirk, L. Scolaro, D. Lorenser, P. D. Robbins, B. A. Wood, C. M. Saunders, and D. D. Sampson, "Imaging of breast cancer with optical coherence tomography needle probes: Feasibility and initial results," IEEE J. Sel. Top. Quantum Electron. **18**(3), 1184–1191 (2012).
104. S. Han, M. V. Sarunic, J. Wu, M. Humayun, and C. Yang, "Handheld forward-imaging needle endoscope for ophthalmic optical coherence tomography inspection," J. Biomed. Opt. **13**(2), 020505 (2008).
105. K. M. Joos and J. H. Shen, "Miniature real-time intraoperative forward-imaging optical coherence tomography probe," Biomed. Opt. Express **4**(8), 1342–1350 (2013).
106. T. Asami, H. Terasaki, Y. Ito, T. Sugita, H. Kaneko, J. Nishiyama, H. Namiki, M. Kobayashi, and N. Nishizawa, "Development of a fiber-optic optical coherence tomography probe for intraocular use," Invest. Ophthalmol. Vis. Sci. **57**(9), OCT568 (2016).
107. C. Song, D. Y. Park, P. L. Gehlbach, S. J. Park, and J. U. Kang, "Fiber-optic OCT sensor guided 'SMART' micro-forceps for microsurgery," Biomed. Opt. Express **4**(7), 1045–1050 (2013).
108. G. W. Cheon, Y. Huang, J. Cha, P. L. Gehlbach, and J. U. Kang, "Accurate real-time depth control for CP-SSOCT distal sensor based handheld microsurgery tools," Biomed. Opt. Express **6**(5), 1942–1953 (2015).
109. M. Balicki, J. H. Han, I. Iordachita, P. Gehlbach, J. Handa, R. Taylor, and J. Kang, "Single Fiber Optical Coherence Tomography Microsurgical Instruments for Computer and Robot-Assisted Retinal Surgery," Med Image Comput Comput Assist Interv **12**(Pt 1), 108–115 (2009).

Biomedical Optics EXPRESS

110. C. Song, P. L. Gehlbach, and J. U. Kang, "Active tremor cancellation by a 'smart' handheld vitreoretinal microsurgical tool using swept source optical coherence tomography," Opt. Express **20**(21), 23414–23421 (2012).
111. S. Yang, M. Balicki, T. S. Wells, R. A. Maclachlan, X. Liu, J. U. Kang, J. T. Handa, R. H. Taylor, and C. N. Riviere, "Improvement of optical coherence tomography using active handheld micromanipulator in vitreoretinal surgery," Conf. Proc. IEEE Eng. Med. Biol. Soc. **2013**, 5674–5677 (2013).
112. H. Yu, J.-H. Shen, R. J. Shah, N. Simaan, and K. M. Joos, "Evaluation of microsurgical tasks with OCT-guided and/or robot-assisted ophthalmic forceps," Biomed. Opt. Express **6**(2), 457–472 (2015).
113. G. Geerling, M. Müller, C. Winter, H. Hoerauf, S. Oelckers, H. Laqua, and R. Birngruber, "Intraoperative 2-dimensional optical coherence tomography as a new tool for anterior segment surgery," Arch. Ophthalmol. **123**(2), 253–257 (2005).
114. J. Probst, D. Hillmann, E. Lankenau, C. Winter, S. Oelckers, P. Koch, and G. Hüttmann, "Optical coherence tomography with online visualization of more than seven rendered volumes per second," J. Biomed. Opt. **15**(2), 26014 (2010).
115. "Haag-Streit Surgical iOCT Product Description." [Online]. Available: http://www.haag-streit-surgical.com/products/ophthalmology/ioctr.html.
116. S. Binder, C. I. Falkner-Radler, C. Hauger, H. Matz, and C. Glittenberg, "Feasibility of intrasurgical spectral-domain optical coherence tomography," Retina **31**(7), 1332–1336 (2011).
117. Y. K. Tao, S. K. Srivastava, and J. P. Ehlers, "Microscope-integrated intraoperative OCT with electrically tunable focus and heads-up display for imaging of ophthalmic surgical maneuvers," Biomed. Opt. Express **5**(6), 1877–1885 (2014).
118. J. P. Ehlers, J. Goshe, W. J. Dupps, P. K. Kaiser, R. P. Singh, R. Gans, J. Eisengart, and S. K. Srivastava, "Determination of Feasibility and Utility of Microscope-Integrated Optical Coherence Tomography During Ophthalmic Surgery: the DISCOVER Study RESCAN Results," JAMA Ophthalmol. **133**(10), 1124–1132 (2015).
119. "Zeiss Rescan 700 Technical Specifications." [Online]. Available: https://applications.zeiss.com/C1257BB3003850AB/0/765054E5AE83DFC6C1257A29005CDCB6/$FILE/OPMI_LUMERA700_RESCAN700_SUR6731_RevB_Final_92316.pdf
120. "Leica Microsystems EnFocus Technical Specifications." [Online]. Available: http://www.leica-microsystems.com/products/optical-coherence-tomography-oct/details/product/enfocus/.
121. P. Hahn, O. Carrasco-Zevallos, D. Cunefare, J. Migacz, S. Farsiu, J. A. Izatt, and C. A. Toth, "Intrasurgical Human Retinal Imaging With Manual Instrument Tracking Using a Microscope-Integrated Spectral-Domain Optical Coherence Tomography Device," Transl. Vis. Sci. Technol. **4**(4), 1–9 (2015).
122. O. M. Carrasco-Zevallos, B. Keller, C. Viehland, L. Shen, G. Waterman, B. Todorich, C. Shieh, P. Hahn, A. N. Kuo, C. A. Toth, and J. A. Izatt, "Live volumetric (4D) visualization and guidance of in vivo human ophthalmic microsurgery with intra-operative optical coherence tomography," Sci. Rep. **6**, 31689 2016.
123. J. P. Ehlers, P. K. Kaiser, and S. K. Srivastava, "Intraoperative optical coherence tomography using the RESCAN 700: preliminary results from the DISCOVER study," Br. J. Ophthalmol. **98**(10), 1329–1332 (2014).
124. M. Pfau, S. Michels, S. Binder, and M. D. Becker, "Clinical Experience With the First Commercially Available Intraoperative Optical Coherence Tomography System," Ophthalmic Surg. Lasers Imaging Retina **46**(10), 1001–1008 (2015).
125. J. P. Ehlers, Y. K. Tao, S. Farsiu, R. Maldonado, J. A. Izatt, and C. A. Toth, "Integration of a spectral domain optical coherence tomography system into a surgical microscope for intraoperative imaging," Invest. Ophthalmol. Vis. Sci. **52**(6), 3153–3159 (2011).
126. J. P. Ehlers, Y. K. Tao, S. Farsiu, R. Maldonado, J. A. Izatt, and C. A. Toth, "Visualization of Real-Time Intraoperative Maneuvers with a Microscope-Mounted Spectral Domain Optical Coherence Tomography System," Retina **33**(1), 232–236 (2013).
127. P. Hahn, J. Migacz, R. O'Connell, J. A. Izatt, and C. A. Toth, "Unprocessed real-time imaging of vitreoretinal surgical maneuvers using a microscope-integrated spectral-domain optical coherence tomography system," Graefes Arch. Clin. Exp. Ophthalmol. **251**(1), 213–220 (2013).
128. J. P. Ehlers, S. K. Srivastava, D. Feiler, A. I. Noonan, A. M. Rollins, and Y. K. Tao, "Integrative advances for OCT-guided ophthalmic surgery and intraoperative OCT: microscope integration, surgical instrumentation, and heads-up display surgeon feedback," PLoS One **9**(8), e105224 (2014).
129. C. I. Falkner-Radler, C. Glittenberg, M. Gabriel, and S. Binder, "Intrasurgical Microscope-Integrated Spectral Domain Optical Coherence Tomography Assisted Membrane Peeling," Retina **35**(10), 2100–2106 (2015).
130. T. Just, E. Lankenau, G. Hüttmann, and H. W. Pau, "Intra-operative application of optical coherence tomography with an operating microscope," J. Laryngol. Otol. **123**(9), 1027–1030 (2009).
131. S. Siebelmann, P. Steven, D. Hos, G. Hüttmann, E. Lankenau, B. Bachmann, and C. Cursiefen, "Advantages of microscope-integrated intraoperative online optical coherence tomography: usage in Boston keratoprosthesis type I surgery," J. Biomed. Opt. **21**(1), 016005 (2016).
132. A. Saad, E. Guilbert, A. Grise-Dulac, P. Sabatier, and D. Gatinel, "Intraoperative OCT-Assisted DMEK: 14 Consecutive Cases," Cornea **34**(7), 802–807 (2015).
133. Y. K. Tao, J. P. Ehlers, C. A. Toth, and J. A. Izatt, "Visualization of Vitreoretinal Surgical Manipulations Using Intraoperative Spectral Domain Optical Coherence Tomography," Proc. SPIE **7889**, 78890F (2011).
134. "NVIDIA CUDA." [Online]. Available: http://www.nvidia.com/object/cuda_home_new.html.

Biomedical Optics EXPRESS

135. Y. Jian, K. Wong, and M. V. Sarunic, "Graphics processing unit accelerated optical coherence tomography processing at megahertz axial scan rate and high resolution video rate volumetric rendering," J. Biomed. Opt. **18**(2), 026002 (2013).
136. B. Keller, O. M. Carrasco-Zevallos, D. Nankivil, A. N. Kuo, and J. A. Izatt, "Real-time Acquisition, Processing, and 3D Visualization of Anterior Segment Swept Source Optical Coherence Tomography (SSOCT) at 10 volumes (275 MVoxels) per second," Invest. Ophthalmol. Vis. Sci. **55**, 1631 (2014).
137. C. Viehland, B. Keller, O. M. Carrasco-Zevallos, D. Nankivil, L. Shen, S. Mangalesh, T. Viet, A. N. Kuo, C. A. Toth, and J. A. Izatt, "Enhanced volumetric visualization for real time 4D intraoperative ophthalmic swept-source OCT," Biomed. Opt. Express **7**(5), 1815–1829 (2016).
138. K. Zhang and J. U. Kang, "Graphics processing unit accelerated non-uniform fast Fourier transform for ultrahigh-speed, real-time Fourier-domain OCT," Opt. Express **18**(22), 23472–23487 (2010).
139. K. Zhang and J. U. Kang, "Real-time intraoperative 4D full-range FD-OCT based on the dual graphics processing units architecture for microsurgery guidance," Biomed. Opt. Express **2**(4), 764–770 (2011).
140. J. U. Kang, Y. Huang, K. Zhang, Z. Ibrahim, J. Cha, W. P. A. Lee, G. Brandacher, and P. L. Gehlbach, "Real-time three-dimensional Fourier-domain optical coherence tomography video image guided microsurgeries," J. Biomed. Opt. **17**(8), 081403 (2012).
141. Y. Huang, Z. Ibrahim, D. Tong, S. Zhu, Q. Mao, J. Pang, W. P. Andree Lee, G. Brandacher, and J. U. Kang, "Microvascular anastomosis guidance and evaluation using real-time three-dimensional Fourier-domain Doppler optical coherence tomography," J. Biomed. Opt. **18**(11), 111404 (2013).
142. X. Li, L. Wei, X. Dong, P. Huang, C. Zhang, Y. He, G. Shi, and Y. Zhang, "Microscope-integrated optical coherence tomography for image-aided positioning of glaucoma surgery," J. Biomed. Opt. **20**(7), 076001 (2015).
143. O. M. Carrasco-Zevallos, B. Keller, C. Viehland, P. Hahn, A. Kuo, P. Desouza, C. A. Toth, and J. A. Izatt, "Real-time 4D visualization of surgical maneuvers with 100 kHz swept-source microscope integrated optical coherence tomography (MIOCT) in model eyes," Invest. Ophthalmol. Vis. Sci. **55**, 1633 (2014).
144. L. Shen, O. Carrasco-Zevallos, B. Keller, C. Viehland, G. Waterman, P. S. Hahn, A. N. Kuo, C. A. Toth, and J. A. Izatt, "Novel microscope-integrated stereoscopic heads-up display for intrasurgical optical coherence tomography," Biomed. Opt. Express **7**(5), 1711–1726 (2016).
145. O. M. Carrasco-Zevallos, B. Keller, C. Viehland, L. Shen, G. Waterman, C. Chukwurah, P. Hahn, A. N. Kuo, C. A. Toth, and J. A. Izatt, "Real-time 4D stereoscopic visualization of human opthalmic surgery with swept-source microscope integrated optical coherence tomography," Invest. Ophthalmol. Vis. Sci. **56**, 4085 (2015).
146. O. M. Carrasco-Zevallos, B. Keller, C. Viehland, L. Shen, M. I. Seider, J. A. Izatt, and C. A. Toth, "Optical Coherence Tomography for Retinal Surgery: Perioperative Analysis to Real-Time Four-Dimensional Image-Guided Surgery," Invest. Ophthalmol. Vis. Sci. **57**(9), OCT37–OCT50 (2016).
147. S. A. Boppart, J. M. Herrmann, C. Pitris, D. L. Stamper, M. E. Brezinski, and J. G. Fujimoto, "Real-time optical coherence tomography for minimally invasive imaging of prostate ablation," Comput. Aided Surg. **6**(2), 94–103 (2001).
148. A. V. Shakhov, A. B. Terentjeva, V. A. Kamensky, L. B. Snopova, V. M. Gelikonov, F. I. Feldchtein, and A. M. Sergeev, "Optical coherence tomography monitoring for laser surgery of laryngeal carcinoma," J. Surg. Oncol. **77**(4), 253–258 (2001).
149. K. E. Donaldson, R. Braga-Mele, F. Cabot, R. Davidson, D. K. Dhaliwal, R. Hamilton, M. Jackson, L. Patterson, K. Stonecipher, and S. H. Yoo; ASCRS Refractive Cataract Surgery Subcommittee, "Femtosecond laser-assisted cataract surgery," J. Cataract Refract. Surg. **39**(11), 1753–1763 (2013).
150. B. Y. C. Leung, P. J. L. Webster, J. M. Fraser, and V. X. D. Yang, "Real-time guidance of thermal and ultrashort pulsed laser ablation in hard tissue using inline coherent imaging," Lasers Surg. Med. **44**(3), 249–256 (2012).
151. Y. Zhang, T. Pfeiffer, M. Weller, W. Wieser, R. Huber, J. Raczkowsky, J. Schipper, H. Wörn, and T. Klenzner, "Optical Coherence Tomography Guided Laser Cochleostomy: Towards the Accuracy on Tens of Micrometer Scale," BioMed Res. Int. **2014**, 251814 (2014).
152. F.-Y. Chang, M.-T. Tsai, Z.-Y. Wang, C.-K. Chi, C.-K. Lee, C.-H. Yang, M.-C. Chan, and Y.-J. Lee, "Optical coherence tomography-guided laser microsurgery for blood coagulation with continuous-wave laser diode," Sci. Rep. **5**, 16739 (2015).
153. Z. Li, J. H. Shen, J. A. Kozub, R. Prasad, P. Lu, and K. M. Joos, "Miniature Forward-Imaging B-Scan Optical Coherence Tomography Probe to Guide Real-Time Laser Ablation," Lasers Surg. Med. **46**(3), 193–202 (2014).
154. G. D. Aaker, L. Gracia, J. S. Myung, V. Borcherding, J. R. Banfelder, D. J. D'Amico, and S. Kiss, "Volumetric three-dimensional reconstruction and segmentation of spectral-domain OCT," Ophthalmic Surg. Lasers Imaging **42**(4 Suppl), S116–S120 (2011).
155. J. P. Schulze, C. Schulze-Döbold, A. Erginay, and R. Tadayoni, "Visualization of three-dimensional ultra-high resolution OCT in virtual reality," Stud. Health Technol. Inform. **184**, 387–391 (2013).
156. I. Kozak, P. Banerjee, J. Luo, and C. Luciano, "Virtual reality simulator for vitreoretinal surgery using integrated OCT data," Clin. Ophthalmol. **8**, 669–672 (2014).
157. L. Shen, B. Keller, O. M. Carrasco-Zevallos, C. Viehland, P. Bhullar, G. Waterman, A. N. Kuo, C. A. Toth, and J. A. Izatt, "Oculus rift® as a head tracking, stereoscopic head-mounted display for intraoperative OCT in ophthalmic surgery," Invest. Ophthalmol. Vis. Sci. **57**, 1701 (2016).
158. M. Draelos, B. Keller, O. M. Carrasco-Zevallos, A. Kuo, and J. Izatt, "Seeing Is Believing: Real-Time Visualization and Interaction with Optical Coherence Tomography Volumes in Immersive Virtual Reality," *presented at Photonics West SPIE BiOS*, 2017.

Biomedical Optics EXPRESS

159. M. T. El-Haddad and Y. K. Tao, "Automated stereo vision instrument tracking for intraoperative OCT guided anterior segment ophthalmic surgical maneuvers," Biomed. Opt. Express **6**(8), 3014–3031 (2015).
160. M. T. El-Haddad and Y. K. Tao, "Real-time dynamic depth tracking for arbitrarily long range OCT imaging and surgical instrument tracking using a Fourier domain optical delay line," Invest. Ophthalmol. Vis. Sci. **56**(7), 4089 (2015).
161. H. Yu, J. H. Shen, K. M. Joos, and N. Simaan, "Design, calibration and preliminary testing of a robotic telemanipulator for OCT guided retinal surgery," *Proc. IEEE Int. Conf. Robot. Autom.*, pp. 225–231, 2013.
162. T. S. Ralston, S. G. Adie, D. L. Marks, S. A. Boppart, and P. S. Carney, "Cross-validation of interferometric synthetic aperture microscopy and optical coherence tomography," Opt. Lett. **35**(10), 1683–1685 (2010).
163. F. A. South, E. J. Chaney, M. Marjanovic, S. G. Adie, and S. A. Boppart, "Differentiation of ex vivo human breast tissue using polarization-sensitive optical coherence tomography," Biomed. Opt. Express **5**(10), 3417–3426 (2014).
164. C. Kut, K. L. Chaichana, J. Xi, S. M. Raza, X. Ye, E. R. McVeigh, F. J. Rodriguez, A. Quiñones-Hinojosa, and X. Li, "Detection of human brain cancer infiltration ex vivo and in vivo using quantitative optical coherence tomography," Sci. Transl. Med. **7**, 292 (2015).
165. D. Y. Kim, J. Fingler, R. J. Zawadzki, S. S. Park, L. S. Morse, D. M. Schwartz, S. E. Fraser, and J. S. Werner, "Optical imaging of the chorioretinal vasculature in the living human eye," Proc. Natl. Acad. Sci. U.S.A. **110**(35), 14354–14359 (2013).
166. Y. Jia, S. T. Bailey, T. S. Hwang, S. M. McClintic, S. S. Gao, M. E. Pennesi, C. J. Flaxel, A. K. Lauer, D. J. Wilson, J. Hornegger, J. G. Fujimoto, and D. Huang, "Quantitative optical coherence tomography angiography of vascular abnormalities in the living human eye," Proc. Natl. Acad. Sci. U.S.A. **112**(18), E2395–E2402 (2015).
167. K. K. C. Lee, A. Mariampillai, J. X. Z. Yu, D. W. Cadotte, B. C. Wilson, B. A. Standish, and V. X. D. Yang, "Real-time speckle variance swept-source optical coherence tomography using a graphics processing unit," Biomed. Opt. Express **3**(7), 1557–1564 (2012).
168. Y. Watanabe, Y. Takahashi, and H. Numazawa, "Graphics processing unit accelerated intensity-based optical coherence tomography angiography using differential frames with real-time motion correction," J. Biomed. Opt. **19**(2), 021105 (2013).
169. J. Xu, K. Wong, Y. Jian, and M. V. Sarunic, "Real-time acquisition and display of flow contrast using speckle variance optical coherence tomography in a graphics processing unit," J. Biomed. Opt. **19**(2), 026001 (2014).
170. C. D. Lu, A. J. Witkin, N. K. Waheed, B. Postsaid, J. J. Liu, E. M. Moult, V. Jayaraman, K. Chan, J. S. Duker, and J. G. Fujimoto, "Ultrahigh Speed Ophthalmic Surgical OCT for Intraoperative OCT Angiography and Widefield Imaging," *ARVO Meet. Abstr.*, vol. 57, no. 12, 2016.
171. X. Chen, C. Viehland, O. M. Carrasco-Zevallos, B. Keller, L. Vajzovic, J. A. Izatt, and C. A. Toth, "Intraoperative Optical Coherence Tomography Angiography in Young Children with Retinal Vascular Disease," JAMA Ophthalmol. In press.
172. S. Yazdanfar, M. Kulkarni, and J. Izatt, "High resolution imaging of in vivo cardiac dynamics using color Doppler optical coherence tomography," Opt. Express **1**(13), 424–431 (1997).
173. R. A. Leitgeb, R. M. Werkmeister, C. Blatter, and L. Schmetterer, "Doppler Optical Coherence Tomography," Prog. Retin. Eye Res. **41**(1), 26–43 (2014).
174. C. C. Wykoff, A. M. Berrocal, A. C. Schefler, S. R. Uhlhorn, M. Ruggeri, and D. Hess, "Intraoperative OCT of a full-thickness macular hole before and after internal limiting membrane peeling," Ophthalmic Surg. Lasers Imaging **41**(1), 7–11 (2010).
175. J. P. Ehlers, K. Kernstine, S. Farsiu, N. Sarin, R. Maldonado, and C. A. Toth, "Analysis of pars plana vitrectomy for optic pit-related maculopathy with intraoperative optical coherence tomography: a possible connection with the vitreous cavity," Arch. Ophthalmol. **129**(11), 1483–1486 (2011).
176. D. H. Nam, P. J. Desouza, P. Hahn, V. Tai, M. B. Sevilla, D. Tran-Viet, D. Cunefare, S. Farsiu, J. A. Izatt, and C. A. Toth, "Intraoperative Spectral Domain Optical Coherence Tomography Imaging After Internal Limiting Membrane Peeling in Idiopathic Epiretinal Membrane with Connecting Strands," Retina **35**(8), 1622–1630 (2015).
177. J. P. Ehlers, D. Xu, P. K. Kaiser, R. P. Singh, and S. K. Srivastava, "Intrasurgical dynamics of macular hole surgery: An Assessment of Surgery-Induced Ultrastructural Alterations with Intraoperative Optical Coherence Tomography," Retina **34**(2), 213–221 (2014).
178. J. P. Ehlers, T. Tam, P. K. Kaiser, D. F. Martin, G. M. Smith, and S. K. Srivastava, "Utility of Intraoperative Optical Coherence Tomography During Vitrectomy Surgery for Vitreomacular Traction syndrome," Retina **34**(7), 1341–1346 (2014).
179. J. P. Ehlers, M. P. Ohr, P. K. Kaiser, and S. K. Srivastava, "Novel microarchitectural dynamics in rhegmatogenous retinal detachments identified with intraoperative optical coherence tomography," Retina **33**(7), 1428–1434 (2013).
180. J. P. Ehlers, J. Han, D. Petkovsek, P. K. Kaiser, R. P. Singh, and S. K. Srivastava, "Membrane Peeling-Induced Retinal Alterations on Intraoperative OCT in Vitreomacular Interface Disorders From the PIONEER Study," Invest. Ophthalmol. Vis. Sci. **56**(12), 7324–7330 (2015).
181. C. Jayadev, S. Dabir, A. Vinekar, U. Shah, T. Vaid, and N. K. Yadav, "Microscope-integrated optical coherence tomography: A new surgical tool in vitreoretinal surgery," Indian J. Ophthalmol. **63**(5), 399–403 (2015).

Biomedical Optics EXPRESS

182. M. I. Seider, O. M. Carrasco-Zevallos, B. Keller, C. A. Toth, and J. A. Izatt, "Real-Time Swept-Source Microscope-Integrated versus Hand-Held Spectral Domain Optical Coherence Tomography during Macular Hole Surgery," Invest. Ophthalmol. Vis. Sci. **56**, 4084 (2015).
183. D. S. Grewal, O. M. Carrasco-Zevallos, R. Gunther, J. A. Izatt, C. A. Toth, and P. Hahn, "Intra-operative microscope-integrated swept-source optical coherence tomography guided placement of Argus II retinal prosthesis," *Acta Ophthalmol.*, vol. ePub ahead of print, 2016.
184. D. S. Grewal, P. Bhullar, N. D. Pasricha, O. M. Carrasco-Zevallos, C. Viehland, B. Keller, L. Shen, J. A. Izatt, A. N. Kuo, C. A. Toth, and P. Mruthyunjaya, "Intraoperative 4-Dimensional Microscope-Integrated Optical Coherence Tomography – Guided 27-Gauge Transvitreal Choroidal Biopsy for Choroidal Melanoma Case Reports and Surgical Technique," *Retina*, no. ePub ahea of print, pp. 1–4, 2016.
185. P. B. Knecht, C. Kaufmann, M. N. Menke, S. L. Watson, and M. M. Bosch, "Use of intraoperative fourier-domain anterior segment optical coherence tomography during descemet stripping endothelial keratoplasty," Am. J. Ophthalmol. **150**(3), 360–365 (2010).
186. V. Scorcia, M. Busin, A. Lucisano, J. Beltz, A. Carta, and G. Scorcia, "Anterior segment optical coherence tomography-guided big-bubble technique," Ophthalmology **120**(3), 471–476 (2013).
187. J. Au, J. Goshe, W. J. Dupps, Jr., S. K. Srivastava, and J. P. Ehlers, "Intraoperative Optical Coherence Tomography for Enhanced Depth Visualization in Deep Anterior Lamellar Keratoplasty From the PIONEER Study," Cornea **34**(9), 1039–1043 (2015).
188. P. Steven, C. Le Blanc, K. Velten, E. Lankenau, M. Krug, S. Oelckers, L. M. Heindl, U. Gehlsen, G. Hüttmann, and C. Cursiefen, "Optimizing descemet membrane endothelial keratoplasty using intraoperative optical coherence tomography," JAMA Ophthalmol. **131**(9), 1135–1142 (2013).
189. P. Steven, C. Le Blanc, E. Lankenau, M. Krug, S. Oelckers, L. M. Heindl, U. Gehlsen, G. Huettmann, and C. Cursiefen, "Optimising deep anterior lamellar keratoplasty (DALK) using intraoperative online optical coherence tomography (iOCT)," Br. J. Ophthalmol. **2013**, 304585 (2014).
190. N. D. Pasricha, C. Shieh, O. M. Carrasco-Zevallos, B. Keller, J. A. Izatt, C. A. Toth, and A. N. Kuo, "Real-Time Microscope-Integrated OCT to Improve Visualization in DSAEK for Advanced Bullous Keratopathy," Cornea **34**(12), 1606–1610 (2015).
191. N. D. Pasricha, P. Bhullar, C. Shieh, O. M. Carrasco-Zevallos, B. Keller, J. A. Izatt, C. A. Toth, S. F. Freedman, and A. N. Kuo, "4D Microscope-integrated OCT to enhance visualization in strabismus surgery," J. Pediatr. Ophthalmol. Strabismus. In press.
192. N. D. Pasricha, P. Bhullar, C. Shieh, C. Viehland, O. M. Carrasco-Zevallos, B. Keller, J. A. Izatt, C. A. Toth, P. Challa, and A. N. Kuo, "4D Microscope-Integrated OCT to Enhance Visualization in Glaucoma Surgeries," Indian J. Ophthalmol. In press.
193. T. V. Roberts, M. Lawless, S. J. Bali, C. Hodge, and G. Sutton, "Surgical outcomes and safety of femtosecond laser cataract surgery: a prospective study of 1500 consecutive cases," Ophthalmology **120**(2), 227–233 (2013).
194. R. G. Abell, E. Darian-Smith, J. B. Kan, P. L. Allen, S. Y. P. Ewe, and B. J. Vote, "Femtosecond laser-assisted cataract surgery versus standard phacoemulsification cataract surgery: outcomes and safety in more than 4000 cases at a single center," J. Cataract Refract. Surg. **41**(1), 47–52 (2015).
195. F. T. Nguyen, A. M. Zysk, E. J. Chaney, J. G. Kotynek, U. J. Oliphant, F. J. Bellafiore, K. M. Rowland, P. A. Johnson, and S. A. Boppart, "Intraoperative evaluation of breast tumor margins with optical coherence tomography," Cancer Res. **69**(22), 8790–8796 (2009).
196. F. T. Nguyen, A. M. Zysk, E. J. Chaney, S. G. Adie, J. G. Kotynek, U. J. Oliphant, F. J. Bellafiore, K. M. Rowland, P. A. Johnson, and S. A. Boppart, "Optical coherence tomography: the intraoperative assessment of lymph nodes in breast cancer," IEEE Eng. Med. Biol. Mag. **29**(2), 63–70 (2010).
197. R. M. Nolan, S. G. Adie, M. Marjanovic, E. J. Chaney, F. A. South, G. L. Monroy, N. D. Shemonski, S. J. Erickson-Bhatt, R. L. Shelton, A. J. Bower, D. G. Simpson, K. A. Cradock, Z. G. Liu, P. S. Ray, and S. A. Boppart, "Intraoperative optical coherence tomography for assessing human lymph nodes for metastatic cancer," BMC Cancer **16**(1), 144 (2016).
198. L. P. Hariri, M. Mino-Kenudson, M. Lanuti, A. J. Miller, E. J. Mark, and M. J. Suter, "Diagnosing lung carcinomas with optical coherence tomography," Ann. Am. Thorac. Soc. **12**(2), 193–201 (2015).
199. Z. Hamdoon, W. Jerjes, G. McKenzie, A. Jay, and C. Hopper, "Optical coherence tomography in the assessment of oral squamous cell carcinoma resection margins," Photodiagn. Photodyn. Ther. **13**, 211–217 (2016).
200. H. S. Lee, S. W. Shin, J. K. Bae, W. G. Jung, S. W. Kim, C. Oak, B. K. Chun, Y.-C. Ahn, B.-J. Lee, and K. D. Lee, "Preliminary study of optical coherence tomography imaging to identify microscopic extrathyroidal extension in patients with papillary thyroid carcinoma," Lasers Surg. Med. **48**(4), 371–376 (2016).
201. A. Dubois and A. C. Boccara, "Full-field Optical Coherence Microscopy," in *Optical Coherence Tomography: Technology and Applications*, W. Dexler and J. G. Fujimoto, Eds. 2008, pp. 565–591.
202. M. Jain, B. D. Robinson, B. Salamoon, O. Thouvenin, C. Boccara, and S. Mukherjee, "Rapid evaluation of fresh ex vivo kidney tissue with full-field optical coherence tomography," J. Pathol. Inform. **6**(1), 53 (2015).
203. T. Maier, D. Kulichová, T. Ruzicka, C. Kunte, and C. Berking, "Ex vivo high-definition optical coherence tomography of basal cell carcinoma compared to frozen-section histology in micrographic surgery: a pilot study," J. Eur. Acad. Dermatol. Venereol. **28**(1), 80–85 (2014).
204. J. Lopater, P. Colin, F. Beuvon, M. Sibony, E. Dalimier, F. Cornud, and N. B. Delongchamps, "Real-time cancer diagnosis during prostate biopsy: ex vivo evaluation of full-field optical coherence tomography (FFOCT) imaging on biopsy cores," World J. Urol. **34**(2), 237–243 (2016).

Biomedical Optics EXPRESS

205. O. M. Carrasco-Zevallos, B. Keller, C. Viehland, L. Shen, B. Todorich, C. Shieh, A. Kuo, C. Toth, and J. A. Izatt, "4D microscope-integrated OCT improves accuracy of ophthalmic surgical maneuvers," Proc. SPIE **9693**, 969306 (2016).
206. N. D. Pasricha, C. Shieh, O. M. Carrasco-Zevallos, B. Keller, D. Cunefare, J. S. Mehta, S. Farsiu, J. A. Izatt, C. A. Toth, and A. N. Kuo, "Needle Depth and Big-Bubble Success in Deep Anterior Lamellar Keratoplasty: An Ex Vivo Microscope-Integrated OCT Study," Cornea **35**(11), 1471–1477 (2016).
207. P. Bhullar, O. M. Carrasco-Zevallos, A. Dandridge, N. D. Pasricha, B. Keller, L. Shen, J. A. Izatt, C. A. Toth, and A. N. Kuo, "Intraocular pressure and big bubble diameter in deep anterior lamellar keratoplasty: an ex vivo microscope-integrated OCT with heads-up display study," *Submitted*.

1. Clinical motivation for intraoperative OCT

Microsurgery may be defined as surgery performed at the sub-millimeter scale and, due to its minimally invasive nature, has been adopted for a wide array of surgical disciplines, including neurosurgery and ophthalmic surgery [1]. The use of microscopes during early microsurgery not only improved efficacy but also facilitated the rapid development of new techniques made possible by magnifying the surgeon's view [1–4]. The operating microscope, however, has not changed significantly since its first use in microsurgery in the 1930's [5], and it currently limits the surgeon's view to an *en face* perspective. As a result, surgeons operating though a modern microscope must infer depth information using stereoscopy and cannot visualize sub-surface structures non-invasively. This sub-optimal intraoperative visualization may limit the surgeon's ability to accurately position instruments axially [6] and may compromise the surgeon's assessment of surgical endpoints [7]. Moreover, a lack of tomographic intraoperative visualization hinders other surgical disciplines outside of microsurgery, such as tumor resections during which the inability to evaluate the sub-surface tissue structure could result in improper margin assessments and reduced patient survival rates [8–11].

The development and clinical adoption of tomographic imaging modalities, such as computed tomography (CT), magnetic resonance imaging (MRI), and ultrasound, have transformed pre- and post-operative management [12–14]. Such modalities are now commonplace for surgical planning, but their intraoperative applications suffer from limited resolution [15,16], patient exposure to ionizing radiation [17,18], and incompatibility with surgical instruments [19,20]. Optical imaging using fluorescent exogenous contrast agents has demonstrated potential for guiding cancer surgery [21,22]. This technology is restricted, however, not only by the need for tumor-specific contrast agents but also by the limited availability of such agents and additional risks associated with their use in patients undergoing surgery [23].

Optical coherence tomography (OCT) [24] is a non-contact imaging modality capable of detecting photons backscattered from tissue with high sensitivity and micrometer-scale spatial resolution. The advent of Fourier-domain detection for OCT [25–28] and confirmation of its sensitivity advantage over time-domain technologies [29–31] facilitated the progression from real-time B-scan imaging [32,33] to real-time volumetric imaging [34]– [36] while preserving OCT's diagnostic potential [37–41]. Consequently, the Fourier-domain OCT revolution of the early 2000's led to increased commercialization [42], widespread clinical adoption of OCT in ophthalmology [43–45], and increasing prominence of OCT in other specialties such as cardiology [46], gastroenterology [47], and cancer imaging [48–51].

The first reports of OCT for perioperative management in the mid-1990's focused on pre-operative planning and post-operative monitoring of ocular surgery [52]. Perioperative OCT has since facilitated the identification of pathologic structures and surgically-induced alterations that are difficult to detect with alternative ophthalmic clinical instruments [53–64]. Initial investigations into OCT's potential for surgical diagnostics in other microsurgeries were also conducted for the first time in the late 1990's [65]. From these studies, investigators determined that intraoperative OCT (iOCT) could be advantageous compared to alternative imaging modalities not only due to its superior resolution, but also because OCT was based on optical communications technology that was more cost-effective and could be readily

Biomedical Optics EXPRESS

integrated into surgical instruments and microscopes. Three key technological developments, in conjunction with the Fourier-domain revolution of the early 2000's [29–31], facilitated the introduction of OCT into the operating suite: handheld OCT (HHOCT) probes [66,67], microscope-integrated OCT (MIOCT) [68–71], and OCT-guided laser surgical modules [72,73].

The aim of this manuscript is to review key intraoperative OCT technologies and their application to various surgical disciplines. This manuscript covers both research prototypes and commercial intraoperative OCT devices, and to differentiate these two classes of devices, all commercial systems are explicitly identified as such for the reminder of the text. Moreover, both devices in the pre-clinical prototype phase of development and devices suitable for large-scale clinical studies are reviewed. Sections 2-5 of the manuscript focus on intraoperative OCT technology and encompass devices suitable for both pre-clinical and clinical studies, while Section 6 discusses salient intraoperative OCT clinical studies and is restricted to devices suitable for such studies.

2. Intraoperative handheld OCT

Due to its physical size and design, conventional tabletop OCT systems require up-right and cooperative patients for imaging [43]. The development of HHOCT probes enabled imaging of patients that are supine, under anesthesia, or unable to maintain the required posture. Boppart *et al.* [66] reported the first forward-imaging handheld OCT probes using a piezoelectric cantilever to translate the light-delivering fiber and scan a focused beam across the sample. The fiber-based scanning mechanism, although compact, limited the field of view and image acquisition rate of the system compared to traditional galvanometer scanned approaches [43]. Galvanometer scanning mirrors were subsequently incorporated into HHOCT and allowed greater speed and flexibility for optical scanning at the cost of increased size and weight of the probe [67]. More recently, the introduction of microelectromechanical (MEMS) devices as compact optical scanners [74,75] to replace galvanometer scanners has resulted in smaller and lighter HHOCT probes [76–78]. In general, however, mirror-based optical scanning probes are larger in size and more suitable for non-invasive surgical imaging (Section 2.1), while fiber-based scanning probes can be made compact enough to be integrated into surgical needles (Section 2.2) and instruments (Section 2.3).

2.1 External intraoperative handheld OCT probes

We first focus on HHOCT probes applied for intraoperative ophthalmic imaging using galvanometer mirror scanners. The handheld design reported by Radhakrishnan *et al.* in 2001 [67] was similar to the ophthalmic HHOCT probe later commercialized by Bioptigen, Inc. (Research Triangle Park, NC) in 2007 [79]. In this design, collimated light was relayed onto galvanometer scanning mirrors and a 4f afocal relay was used to image the beam scanning pivot to the ocular pupil of the subject (Fig. 1(a)). The collimated beam was then focused by the subject's optics for retinal imaging. Alternatively, an additional lens could be added after the 4f relay to scan the anterior eye with a focused beam. The Bioptigen HHOCT employed an 850 nm spectral-domain system that produced tomograms at 17k A-scans/second with an axial resolution of 5 μm. This line rate, in conjunction with fast galvanometer-based scanning, could yield video-rate B-scans with minimal motion artifacts but volumetric acquisition rates were still limited to several seconds. The acquired B-scans and summed voxel projects (SVPs) were processed and displayed in real-time on a computer monitor. During handheld operation, the probe could be angled and translated by the operator to center the scans on the site of interest [80]. Alternatively, the probe could also be situated on a mount for added stability [81,82]. The Bioptigen HHOCT probe was first used for pediatric ocular imaging [7,83–86] and introduced for human intraoperative ophthalmic imaging in 2009 [80]. Similar HHOCT systems from other vendors have since been developed and applied during ophthalmic surgery [87–89].

Biomedical Optics EXPRESS

Outside of ocular surgery, extensive development of probes for other surgical applications has been demonstrated by various research groups. An HHOCT probe employing a similar optical design to [67] was used to image six patients undergoing open knee surgery in 2005 [90]. Another probe using a 1300 nm swept-source laser with a 50 kHz line rate for OCT guidance of vascular anastomosis was demonstrated in 2014 [91] (Fig. 1(b)). A key feature demonstrated in [91] was the incorporation of MEMS scanner [74,75], which had been previously employed in catheter-based OCT systems [92,93] and other HHOCT probes for non-intraoperative use [76–78]. The intraoperative HHOCT probe's size was significantly decreased by using the MEMS scanner, and the probe's functionality was tested during anastomosis performed *in vivo* in a mouse surgical model [91]. Moreover, a contact-based intrasurgical HHOCT probe for tumor margin analysis during human breast surgery was demonstrated in 2015 [94], and a similar probe has since been commercialized by Diagnostic Photonics, Inc [95]. The commercial probe was coupled to a 1300 nm swept-source OCT system and used a MEMS scanner to acquire images with a transverse resolution of ~15 µm over a 9 mm lateral field of view [95]. The longer operating wavelength resulted in poorer axial resolution compared to 850 nm HHOCT for retinal imaging but longer penetration depth, which was beneficial for imaging turbid media such as normal and pathologic breast tissue. Similarly, a recently reported probe also used a 1300 nm swept-source system operating at 100 kHz for intraoperative imaging of pediatric vocal fold lesions [96]. This side-viewing probe employed GRIN lenses, 2.7 mm in diameter and 95-127 mm long, to relay focused light to the sample. The beam was scanned in the transverse plane using a galvanometer mirror pair prior to the GRIN lens relay (Fig. 1(c)). A rotation mount incorporated into this probe also allowed the OCT scan to be optimally positioned without requiring the surgeon to rotate his/her hand. Similar to previous non-ophthalmic probes, the 1300 nm operating central wavelength allowed deeper penetration into highly scattering tissue.

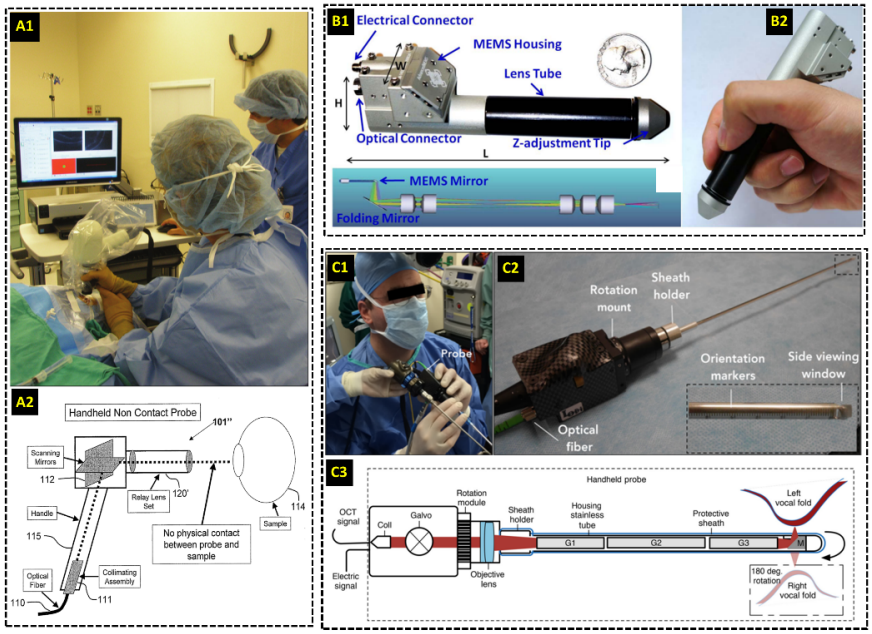

Fig. 1. External intraoperative handheld OCT (HHOCT) probes. (A) Commercial HHOCT probe used for imaging human ocular surgeries. The probe uses galvanometer scanning mirrors and a 4f optical relay to scan the beam across the sample [79]. (B) Compact research-grade HHOCT probe for intraoperative imaging of anastomoses [91]. A MEMS-based mirror scanner reduced the overall footprint of the probe. (C) Intraoperative research-grade HHOCT probe using a long GRIN lens-based relay for imaging of pediatric vocal fold lesions [96].

Biomedical Optics EXPRESS

2.2 Needle-based intraoperative OCT probes

Needle-based probes can bypass opacities and highly scattering tissue that limit the imaging depth range of traditional OCT scanners, thus allowing for deep tissue imaging even in turbid media [66,97,98]. In 2011 a probe incorporating galvanometer scanners and GRIN lens-based relays was reported for stereotactic neurosurgery procedures, in which deep-brain tissues are accessed using long cannulas [99]. The needle probe was 0.74 mm in diameter and could be inserted into cannulas to image structures up to 9.5 cm deep into brain tissue. Galvanometer scanners and an additional lens prior to the GRIN relay were used for optical scanning at the sample plane, resulting in a 0.44 mm lateral field of view, 13 µm lateral resolution, and a frame rate of 100 B-scans/second. Another needle OCT probe also designed for neurosurgical applications employed a bayonet form factor identical to that of other clinically-accepted neurosurgical probes [100]. Optical scanning was achieved by enclosing the fiber in a platinum coil located in between two wires inside of the lumen of the probe. When voltage was applied to the wires, the coil oscillated and transversely displaced the fiber tip prior to a GRIN lens used for focusing. Additionally, needle-based probes were demonstrated for guidance of breast biopsy [101,102] and delineation of breast tumor boundaries [103]. The 23-gauge probe described in [103], in particular, employed a side-imaging strategy in which the focused light was directed orthogonal to the needle (Fig. 2(a)) and transverse optical scanning was achieved by rotating and retracting the probe during imaging.

For ophthalmic surgery, needle-based probes small enough to be inserted into the surgical ports at the pars-plana were used to bypass the optics of the microscope and patient [104], [105]. Transverse scanning in [104] was accomplished using two angle polished and counter rotating GRIN lenses at the distal end of a 21-gauge probe. The inner faces of both GRIN lenses were polished at 15 degrees and separated by an air gap. Refraction at the glass/air surface at the distal end of the first GRIN lens angularly displaced the beam incident on the second GRIN lens, and mechanically rotating the lenses relative to each other resulted in transverse scanning at the sample plane. This scanning mechanism produced a B-scan rate of 0.5 frames/second with 500 A-scans/B-scan and a lateral resolution of 7.6-10.4 µm throughout the scanning range. The probe was tested on cadaver porcine eyes. A more recent intraocular 25-gauge OCT needle probe achieved transverse optical scanning by physically displacing the fiber tip using a customized coil-magnetic oscillator housed within the hand piece of the probe [105] (Fig. 2(b)). A 28-gauge stainless steel tube was driven forward and backward as current in the surrounding coil was alternated, and the axial translation of the steel tube displaced the optical fiber laterally prior to a GRIN lens at the distal end of the probe. The transverse scanning range was 3-4 mm with a lateral resolution of 25-35 µm throughout the scanning range and a B-scans rate of 5 frames/second. The functionality of this probe was evaluated in cadaver porcine eyes. Moreover, a side-imaging 23-gauge OCT probe was demonstrated by Asami *et al.* in 2016 and tested in cadaver porcine eyes and three human retinal surgeries [106]. Using this probe, the researchers successfully imaged various intraoperative maneuvers and subtle surgical structures of interest.

Biomedical Optics EXPRESS

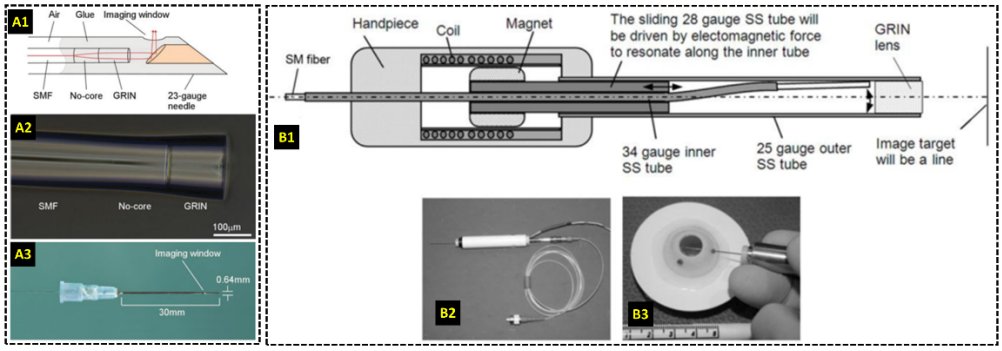

Fig. 2. Research-grade needle-based HHOCT probes for intraoperative imaging. (A) 23-gauge side-viewing probe for imaging of breast cancer [103]. Three-dimensional optical scanning was achieved by rotating and retracting the probe during imaging. (B) 25-gauge forward-imaging probe for imaging during vitreoretinal surgery [105]. Transverse optical scanning was enabled by displacing the fiber tip using a customized coil-magnetic system.

2.3 OCT-integrated surgical instruments

The development of OCT needle-based probes motivated the incorporation of one-dimensional (A-scan only) and two-dimensional OCT imaging into surgical instruments to guarantee alignment of the images with the instrument tip and to provide image-based feedback during surgery. The Kang group at Johns Hopkins University demonstrated that A-scans could be acquired adjacent to the tooltip by mounting a fiber-optic common-path (CP) OCT probe along [107,108] or within [109–111] the shafts of forceps and needles for vitreoretinal surgery (Fig. 3(a)). The reference interference signal was obtained from the partial back-reflection at the distal surface of the CPOCT probe, and the lack of an optical scanning mechanism resulted in a relatively simple and affordable optical design that could potentially be made as a disposable product. In its most recent iteration [108], the probe used a 100 kHz swept-source with a 1060 nm central wavelength, and M-scan images could be acquired and processed with GPU-accelerated software. The OCT probe was primarily used as a single-point axial ranger with micrometer-scale resolution to quantify hand tremor [111] and drive active motion cancellation systems [107,108,110], and to provide ranging feedback for a cooperative robotic surgery platform [109] (discussed in detail in Section 5.2). The Joos group at Vanderbilt University incorporated a needle-based OCT probe [105] capable of B-scan imaging into the shaft of 23-gauge surgical forceps [112] (Fig. 3(b)). This design strategy ensured that the distal ends of the forceps were always visible in the B-scans and minimized OCT shadowing from the instrument, a problem that is frequently encountered in other intraoperative OCT applications (see Sections 3.2 and 3.3).

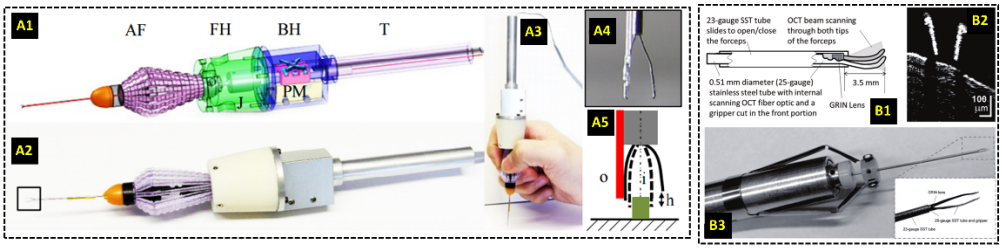

Fig. 3. Surgical instruments with integrated OCT imaging. (A) Surgical forceps with a common path OCT system for axial ranging using A-scans only [107]. (B) OCT probe capable of B-scan imaging integrated into surgical forceps for vitreoretinal surgery [112].

Biomedical Optics EXPRESS

3. Microscope-integrated OCT

A potential limitation of some of the previously described handheld probes is the restriction of imaging to surgical pauses. For ophthalmic surgery in particular, external HHOCT devices need to be placed over the patient's eye during imaging, thus requiring displacement of the surgical microscope and pause in surgery. Needle-based probes could potentially be used during live surgery but may require a surgical assistant to hold the probe and additional instrument ports for access. OCT probes integrated into instruments could be used by the primary surgeon for live surgical imaging, but the functionality of these probes is coupled to the position and orientation of the instrument relative to the tissue of interest, which may not always be optimal for OCT imaging and could compromise image quality. An alternative approach for intraoperative OCT imaging is to integrate the OCT sample arm into the operating microscope required for microsurgeries such as ophthalmic surgery and neurosurgery [68–71]. This design, termed microscope integrated OCT (MIOCT), allows OCT imaging of live surgery without disturbing the surgeon's workflow, and if coupled with immediate OCT feedback to the surgeon, has the potential to impact real-time surgical decision-making.

3.1 Optical designs for microscope-integrated OCT

The first demonstration of MIOCT used a dichroic mirror after the microscope objective to couple the OCT beam onto the optical axis of the operating microscope [69]. With this approach, the OCT and microscope systems did not share any optics and as a result, each optical system could be optimized separately. Coupling the OCT and microscope after the objective, however, reduced the working distance of the microscope, which could potentially obstruct surgical workflow and prevent the system's translation to the human operating suite. More recent MIOCT designs prioritized usability during human surgery by coupling the two modalities prior to the microscope objective at the cost of potentially compromising OCT optical performance [70,71]. In such designs, the OCT beam also traversed any additional optics after the objective, such as contact lenses or additional relays required for retinal imaging.

The first reported MIOCT design for human surgery coupled the OCT beam into the camera port already present in many commercial operating microscopes (Fig. 4(a)) [70,113,114]. A dichroic mirror was used to fold the OCT beam into the path of one the oculars prior to the optical zoom module of the microscope. The beam was then magnified prior to the objective to yield an optimal OCT lateral resolution of 23 µm at the focal plane of the microscope. Since the optical zoom of both modalities were coupled in this design, the MIOCT lateral resolution and field of view could vary from 23 to 47 µm and 4-28 mm, respectively, depending on the microscope magnification setting chosen by the surgeon [70]. An important advantage of this design was the minimal modification to the operating microscope required to integrate the OCT. Coupling the OCT module via an already existing camera port did not alter the height or working distance of the microscope, thereby ensuring that the surgeon's workflow would remain undisturbed. The primary disadvantage of this design, however, was the dependence of OCT lateral resolution and field of view on the microscope's optical zoom, which could result in compromised OCT performance under some magnification settings. This MIOCT design was adopted for the iOCT Camera system for human ocular surgery commercialized by Haag-Streit Surgical [115]. This product received FDA 510(k) clearance in the United States in early 2015.

In an alternative MIOCT design, the two modalities were coupled using a dichroic mirror placed prior to the microscope objective and after the microscope optical zoom module [71], [116–118] (Fig. 4(b)). This approach minimized the number of optical elements shared between the two modalities and decoupled the OCT from microscope's optical zoom. Inserting the dichroic mirror in the infinity space prior to the objective, however, increased the height of the microscope and the distance between the surgical field and microscope

Biomedical Optics EXPRESS

oculars, both of which could negatively impact surgical ergonomics. The OCT beam also had to be magnified prior to the objective to achieve ~15 µm resolution at the microscope focal plane, which required at least one OCT magnifying relay prior to the objective. This need for additional optics could result in an increased scanner footprint and potentially lower optical transmission. A recent MIOCT design, however, employed spherical mirror relays to improve optical transmission at the expense of introducing astigmatism due to the off-axis configuration of the mirrors [117] (Fig. 4(c)). The design strategy of coupling the two modalities directly prior to the microscope objective was implemented in two recently commercialized MIOCT devices for human ocular surgery, the Zeiss RESCAN 700 [119] and the Leica Microsystems EnFocus [120]. These two systems received FDA 510(k) clearance in the United States in 2014 and 2015, respectively.

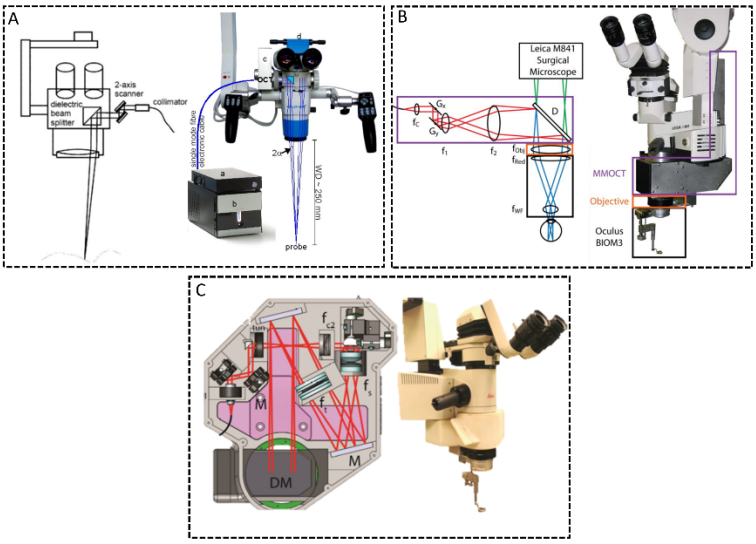

Fig. 4. Optical designs of research-grade MIOCT systems for live surgical imaging. (A) MIOCT scanner coupled onto the camera port of a commercial microscope [70]. The OCT beam traversed through the microscope optical zoom module and the OCT lateral resolution and field of view (FOV) were coupled to the microscope zoom level. (B) MIOCT scanner integrated directly prior to the microscope objective [71]. This design required a telescope to magnify the OCT beam prior to the objective, but the OCT resolution and lateral FOV were independent of the microscope zoom level. (C) Alternative MIOCT design integrated directly prior to the objective and employing reflective elements to improve transmission and a tunable focus lens [117].

Ideally, the MIOCT and operating microscope should be parfocal and coaxial. During surgery, however, the surgeon frequently alters the microscope's lateral and axial position and the region of interest may not be centered laterally or at the OCT focal plane. An optimal MIOCT scanner should adapt to these conditions without altering the surgeon's workflow; therefore, additional functionalities not required for conventional OCT could be useful for live surgical imaging with MIOCT. A previously reported manual tracking system enabled the MIOCT operator to laterally translate the OCT scan within the surgical field [121]. This feature allowed a densely-sampled OCT scan to be re-centered to the site of interest in real-time after lateral translation of the microscope relative to the surgical field. Several MIOCT systems also employed independent OCT refocusing mechanisms in case the surgical field was shifted outside the OCT focus plane [117,121,122]. The electrically-controlled tunable-focus lens incorporated in [117] could also enable automatic focus adjustment. Variations of these features were incorporated in the recently commercialized Zeiss RESCAN 700, which allows the surgeon to translate the OCT scan laterally using a foot-pedal and incorporates

Biomedical Optics EXPRESS

focus control and reference arm tracking to stabilize and optimize the OCT images [118,119,123,124].

The MIOCT scanner may be permanently integrated into the microscope [119] or it may be designed as a modular attachment [115,120] (Fig. 5). This design consideration is primarily relevant for commercialization, since it directly impacts the device's functionality and cost-effectiveness. Two commercial MIOCT systems adopted the modular approach [115,120] and are compatible with multiple microscopes, potentially enabling a single MIOCT scanner to be used in multiple operating suites without needing to relocate the microscope. However, attaching and detaching the device may prolong preparations for surgery and the modular design may have a negative impact on surgical ergonomics (as discussed above). An operating microscope with a permanently integrated MIOCT scanner can be carefully designed such that the addition of OCT minimally alters both the physical appearance of the microscope and surgical ergonomics. Zeiss adopted this strategy for the commercial RESCAN 700 [119]. Such MIOCT scanners, however, cannot be purchased independently of the operating microscope, which could render the device cost-prohibitive.

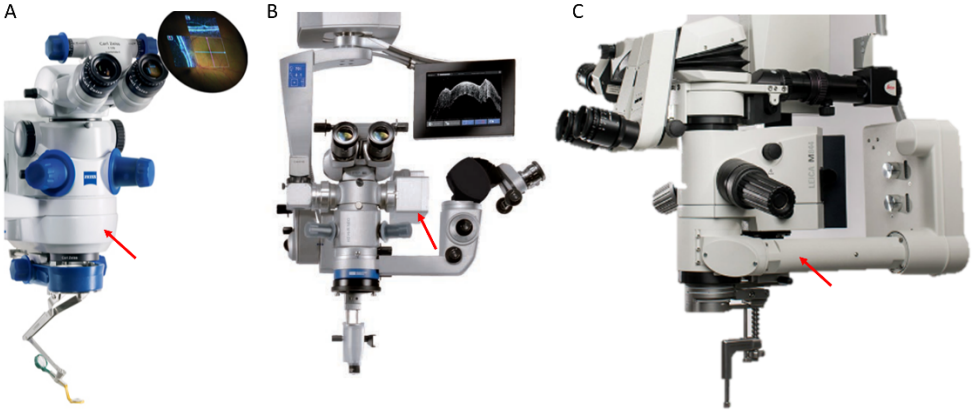

Fig. 5. Commercial MIOCT systems. (A) Zeiss RESCAN 700, FDA cleared in 2014 [119]. This system houses a permanently-integrated OCT scanner coupled directly prior to the microscope objective. (B) Haag-Streit Surgical iOCT, FDA cleared in 2015 [115]. This system uses a modular OCT scanner attached to the camera port of the microscope. (C) Leica Microsystems Bioptigen EnFocus, FDA cleared in 2015 [120]. This system uses a modular OCT scanner attached prior to the objective. Red arrows denote the location of OCT scanners.

3.2 Live two-dimensional microscope-integrated OCT

The majority of previously reported research-grade MIOCT systems used commercial spectral-domain OCT technology that was limited to A-scan rates below 40 kHz [70,71,116,117,121] and as a result, acquisition of densely sampled volumes lasted several seconds and was restricted to surgical pauses. Importantly, these systems also could not render acquired volumetric data in real-time. Imaging of live surgery and surgical maneuvers was thus achieved using continuous high-resolution B-scans that could be generated with minimal motion artifacts [70,71,113,116,117,121,125–131]. This OCT technology was incorporated into the three commercially-available MIOCT scanners for human ocular imaging [115,119,120], and the primary imaging protocol of these systems consisted of two high-resolution orthogonal B-scans or a single high-resolution B-scan centered at the region of interest (Fig. 6(a)). Using the manual tracking feature described in Section 3.1, some of these systems also allowed the B-scans to be manually tracked to the tip of instruments during surgical maneuvers [118,121,122]. Alternatively, multiple (3-5) parallel B-scans spanning the site of interest could be acquired and displayed simultaneously to monitor motion orthogonal to the B-scan axis [123,132] (Fig. 6(b)).

Biomedical Optics EXPRESS

The acquired B-scans in live 2D MIOCT were processed in real-time on a CPU and displayed either on an external monitor or on a heads-up display (HUD) [118,124,128,131] to provide feedback to the surgeon. HUD visualization, discussed in detail in Section 5.1, was particularly important since it allowed the surgeon to alter his/her decision-making in real-time based on the OCT data [118] and to control the OCT scan location with a foot pedal. In addition, to adequately visualize surgical maneuvers on OCT, the instruments used during the maneuvers must be visible and recognizable in the images. The OCT visibility of commonplace instruments for vitreoretinal surgery was tested using a spectral-domain OCT system with a central wavelength of 850 nm [125]. Instruments of various sizes and comprised of different materials were tested. In general, metallic instruments were best visualized in the OCT B-scans but also significantly shadowed the underlying tissue (Fig. 6(a), yellow arrows). Instruments made of silicone and polyamide were still visible in the OCT B-scans but shadowed less. Total shadowing of underlying tissue could hinder OCT visualization of the instrument-tissue point of contact, but this interface could be estimated by acquiring and averaging multiple B-scans acquired adjacent to the shadowed region, a technique termed spatial compounding [126,133]. Prototypes of OCT-compatible surgical instruments were also demonstrated in 2014 [128] and further research and development of such instruments could be catalyzed by the recent commercialization of MIOCT.

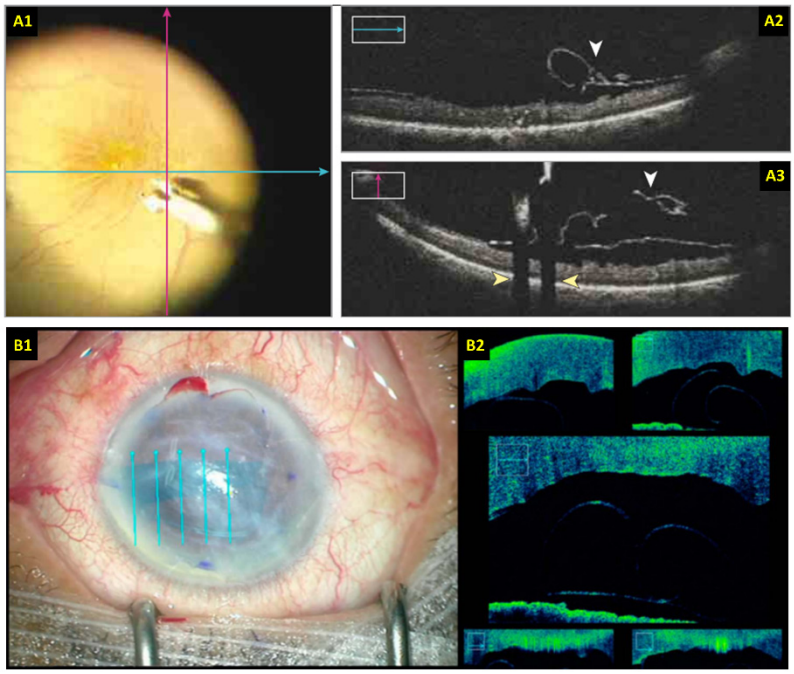

Fig. 6. Surgical imaging with live 2D MIOCT. (A) Retinal surgery imaging protocol using two orthogonal high-resolution B-scans [118]. (B) Anterior eye surgery imaging protocol using five parallel and laterally offset B-scans spanning the area of interest [132]. The B-scan locations are overlaid on the surgical views.

3.3 Live 3D microscope-integrated OCT

The advent of MIOCT technology enabled, for the first time, imaging of live human surgery, including tissue manipulations with various types of instruments. The surgical field, however, is inherently three-dimensional (3D) and as a result, most surgical maneuvers are not constrained to single cross-sectional planes. Thus, live 2D MIOCT techniques had difficulty imaging complete maneuvers and provided limited spatial information and context to the surgeon as the region of interest could move in and out of the imaging plane. The potential

Biomedical Optics EXPRESS

advantages of live 3D OCT for ocular surgery, in particular, were noted in [121,129], but volumetric rendering in these studies was limited to post-processing.

Live 3D intraoperative OCT imaging with MIOCT was in part enabled by acquisition and processing software that leveraged the computational speed of graphics processing units (GPU). GPUs were primarily used for rendering graphics prior to the advent of high level GPU programming languages such as NVIDIA's compute unified device architecture (CUDA) [134]. For OCT in particular, GPU processing became highly desirable as the repetition rate of OCT lasers increased to kilohertz [35,114,135–138] and even megahertz [34], and researchers were no longer able to process OCT data on the CPU in real-time. Moreover, GPUs also allowed real-time volume rendering for visualization and manipulation of OCT 3D and 4D (volumes over time) data. Several research groups explored the potential benefits of 4D OCT for live surgery using surgical phantoms and *ex vivo* animal models. In a series of studies, the Kang group at Johns Hopkins University reported on 4D OCT systems to guide microvascular anastomosis [139–141]. In these studies, the researchers demonstrated a spectral-domain OCT system running at 128 kHz A-scans/second and coupled to a telecentric scanner for imaging. The OCT sample arm beam was displaced away from the pivot of the first galvanometer scanner to induce a phase modulation that allowed estimation of the complex OCT signal for complex conjugate resolved imaging in real-time. This system was used to image mock surgical manipulations at 5 volumes/second using 100x256x1024 (X, Y, Z) voxels over at 3.5x3.5x3.5 mm field of view [139]. Using a similar system in a subsequent study, the imaging speed was increased to 10 volumes/second using 160x80x1024 voxels to image and guide microvascular anastomosis on a rat surgical model [140]. The researchers also reported on a different spectral-domain OCT system with real-time Doppler capabilities to produce blood flow images in conjunction with structural volumes to further improve OCT guidance of anastomosis. While these systems clearly demonstrated the potential of 4D OCT for microsurgical visualization, a lack of integration with an operating microscope designed for human surgery restricted their use to mock surgery. Probst *et al.* [114] in 2010 was the first, to the best our knowledge, to report an MIOCT system with GPU-assisted real-time volumetric imaging and visualization. The researchers demonstrated 4D MIOCT imaging at 7 volumes/second using 300x80x512 voxels on a spectral-domain OCT system running at 210 kHz A-scans/second. Unfortunately, the poor imaging sensitivity (78 dB) of this system restricted its use to surgical phantoms comprised of layers of onion skin. Li *et al.* more recently reported on a swept-source MIOCT system with a central wavelength of 1310 nm to guide anterior eye glaucoma surgery in rabbit eyes [142]. The system speed was 50 kHz A-scans/second and it used a two-GPU software architecture for real-time processing and rendering of volumetric data acquired over 3x3.6x4.2 mm.

4D MIOCT imaging of simulated surgical maneuvers performed with commercial surgical instruments in cadaveric porcine eyes was demonstrated by Carrasco-Zevallos *et al.* in 2014 [143]. This system, together with a custom stereoscopic HUD [144], was translated to the human operating suite in 2015 [122,145,146] and has been used in over 150 human ocular surgeries to date. Using an MIOCT scanner designed for imaging of human ocular surgery [71], the researchers employed a 1040 nm swept-source OCT system running at 100 kHz A-scan rate, which was 3-5 times faster than previous intraoperative OCT systems used in human ocular surgery. Similar to previous 4D OCT systems, the swept-source 4D MIOCT software exploited the speed of GPUs for acquisition, processing, and volumetric rendering [136]. Unlike previous 4D OCT demonstrations, however, the ray casting algorithm used for volume rendering was optimized specifically to enhance the visualization of subtle ocular structures and surgically-induced alterations [137] (Fig. 7(a)). The imaging protocols of 4D MIOCT for human ocular surgery were first determined during preliminary mock surgical trials. In these, the volumetric OCT visualization of commonly used instruments for human ocular surgery was characterized (see Supplementary Information of [122]) (Fig. 7(b)). The instruments tested were constructed of steel, nitinol, silicone, and polyamide. The polymer-

Biomedical Optics EXPRESS

based instruments shadowed less than the steel instruments but were also less reflective. In cases with significant shadowing, however, volumetric imaging provided sufficient spatial context to help the surgeon to interpret the shadowed region, but this system would also benefit greatly from OCT-compatible instruments [128]. The researchers then characterized the tradeoff between lateral sampling density and volumetric imaging speed. The system was found capable of operating at 10 volumes/second using 100x64x688 voxels over a 5x5x3.7 mm field of view during mock surgery in porcine eyes, but the surgeons preferred higher sampling densities to improve the volumetric image quality at the cost of speed during human surgery. The typical human retinal surgery imaging protocol was 300x96x688 voxels at 3.3 volumes/second over 5x5x3.7 mm, and the typical human anterior eye surgery imaging protocol was 500x96x1376 voxels at 0.5 volumes/second over 10x10x7.4 mm. Several other features of the system facilitated its use during live human surgery. A "stream saving" mode in which each OCT volume was saved immediately after acquisition enabled continuous volumetric recording of surgery. Moreover, a manual tracking module similar to that developed by Hahn *et al.* [121] was integrated to compensate for gross lateral motion of the microscope or surgical field.

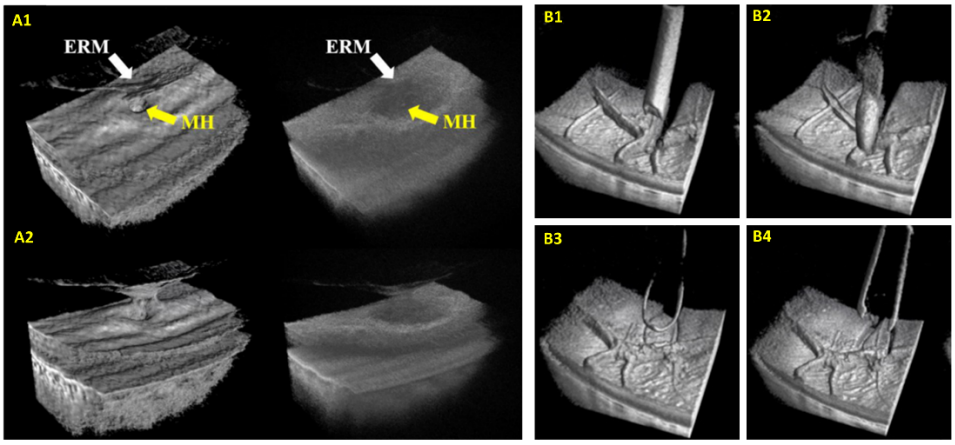

Fig. 7. Surgical imaging with live 3D MIOCT. (A) Real-time enhanced volumetric rendering using GPU-accelerated software. Median filtering and depth-based shading improved visualization of subtle anatomical and pathological structures [137]. Manipulation of the rendering perspective also allowed surgeons to visualize structures from various perspectives. (B) Visualization of commonplace surgical instruments in OCT volumes acquired during porcine eye surgery. ERM: epiretinal membrane, MH: macular hole.

4. OCT-guided laser surgery

The feasibility of OCT guidance and monitoring of laser surgery was first explored in the late 1990's [53,72], and subsequent studies demonstrated the ability of OCT to monitor structural alterations following prostate tissue ablation *in vitro* [147] and laser treatment of laryngeal carcinoma surgery [148]. More recently, Palanker *et al.* in 2010 demonstrated a spectral-domain OCT system incorporated into a femtosecond laser module for human cataract surgery [73] (Fig. 8). In this system, the OCT beam path was coupled to the femtosecond laser path using a dichroic mirror prior to the galvanometer scanning mirrors, and the two modalities shared a focusing objective lens and contact lens placed on the patient's cornea. The OCT system had an axial resolution of 11 µm and sufficiently long imaging depth range to visualize the cornea, anterior chamber, and both anterior and posterior lens surfaces. Using automated software, these surfaces were detected on OCT to ensure the centration of the laser cutting pattern and to avoid inadvertent damage to the cornea or iris. Additionally, intraoperative OCT also allowed depth visualization and more exact placement of corneal relaxing incisions and multi-planar incisions. Intraoperative OCT was particularly

Biomedical Optics EXPRESS

advantageous compared to preoperative OCT since the eye could be deformed during the procedure, rendering the preoperative scans inaccurate. Currently, several commercial femtosecond laser surgery modules feature integrated OCT to aid in the placement of the laser cutting patterns [149].

OCT has also been integrated into non-ophthalmic laser surgical systems to improve the lateral and depth positioning of laser ablation. Intraoperative OCT was used to monitor the ablation depth in bone tissue [150] using M-scans at the incision site during laser application. Another reported OCT system was used to guide laser-based cochleostomy, in which OCT image-based active tracking was implemented for motion compensation and improved 3D positioning of the laser application site [151]. The OCT images were used to estimate both the lateral position of the sample and the depth of the ablation, and this information was used to update the laser pulse duration and position on cadaver cochlea. Additionally, a recent study demonstrated an OCT-guided laser surgical system for blood coagulation [152]. The OCT provided feedback for the laser positioning control loop using M-scans at the site of the ablation. OCT angiography (OCTA) images were also acquired immediately before and after ablation to monitor the laser-induced blood coagulation. Moreover, Li *et al.* recently reported on the integration of OCT into a handheld laser ablation probe to monitor the laser incision depth [153].

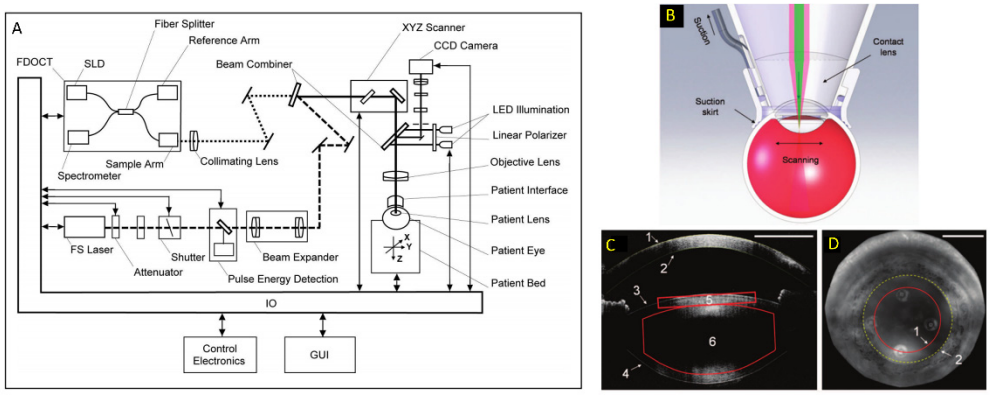

Fig. 8. OCT-guided femtosecond laser surgical module for anterior eye surgery [73]. (A) The two modalities were coupled using a dichroic mirror prior to the scanning mirrors and shared an objective and the contact lens (B) used to deliver light to the surgical site. (C) OCT volumes were used to detect the various tissue surfaces and allowed the surgeon to precisely position the laser cutting pattern and avoid damage to the iris and surrounding structures. (D) Iris camera image denoting the edge of the laser cutting pattern (1) and the pupil boundary determined on OCT (2).

5. OCT enhanced surgeon feedback

5.1 Heads-up displays and OCT visualization

Live OCT imaging is most useful in guiding operations when it provides feedback to the surgeon during surgical manipulation instead of during surgical pauses, and heads-up display (HUDs) technology has emerged to display MIOCT images within the microscope oculars (Fig. 9) and to facilitate real-time OCT feedback. Most reported HUDs used micro-displays to project live 2D OCT images into one [118,119,124,128] or both [131] oculars of the operating microscope. Alternatively, a compact stereoscopic HUD was developed to display live 3D OCT stereo images through the oculars and enhance the surgeon's depth perception of the volumetric data [144]. This HUD employed a spatial multiplexing technique in which only one micro-display was required to relay a stereo pair of OCT volumes to the oculars, thereby decreasing the footprint of the HUD. Compared to some commercially available HUDs [117], the organic light-emitting diode (OLED) micro-display used in the stereo HUD

Biomedical Optics EXPRESS

also offered improved contrast and completely transparent black pixels so that the view of the surgical field was not obscured. In all reports describing MIOCT HUDs, the projected OCT images were overlaid on top of the surgical field and needed to be carefully placed to not obstruct visualization of the regions of interest. As HUD technology progresses, its ability to provide real-time OCT feedback to the surgeon may become crucial for OCT-guided surgery, and recent clinical studies have already suggested surgeons prefer HUDs over external displays for intraoperative OCT visualization [118,124].

An unfortunate limitation of HUDs is the limited resolution, contrast, and field of view available to visualize the OCT images. Beyond HUDs, virtual reality (VR) has become increasingly popular for viewing OCT data sets. Computer Assisted Virtual Environments [154], 3D televisions [155], and stereo microscope-style simulators [156] have been demonstrated utility for presenting OCT images. Immersive head-mounted displays (HMDs) for VR offer even larger fields of view than stereo displays as the wearer can look in any direction. The Oculus Rift by Oculus VR [157] and the Vive by HTC [158] have garnered interest as platforms for OCT data set viewing and manipulation in seated and room-scale VR experiences, respectively, especially for volumetric data sets. These technologies could be useful for pre- and post-postoperative analysis and may be desirable for intraoperative use as intraoperative OCT becomes more commonplace.

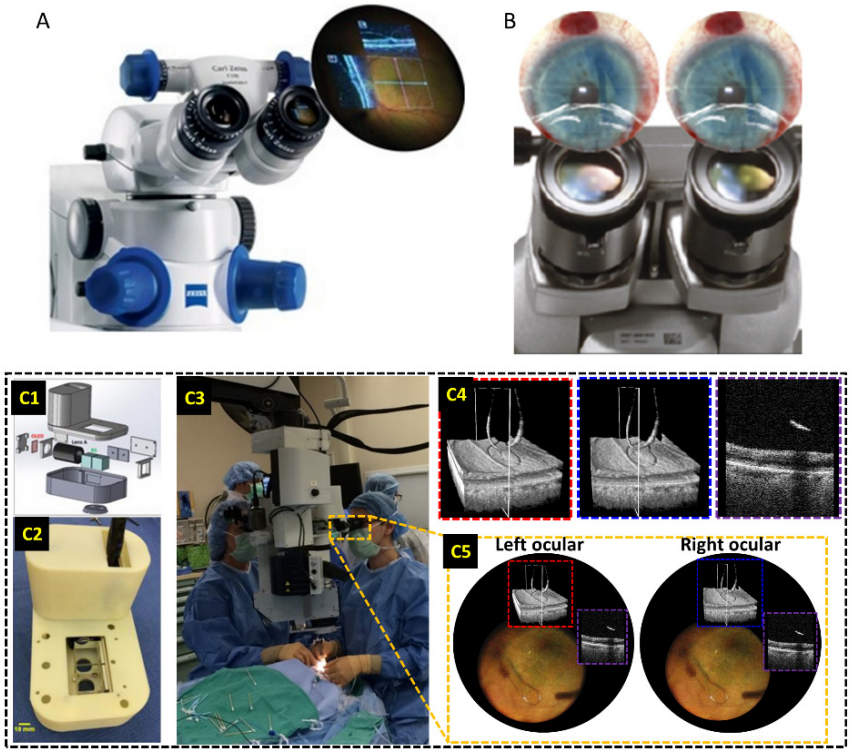

Fig. 9. Heads-up displays (HUD) for intraoperative OCT visualization. (A) Monocular HUD integrated into the commercial Zeiss RESCAN 700 [119]. (B) Binocular HUD integrated into the commercial Haag-Streit Surgical iOCT [115]. Both (A) and (B) are used to project live B-scans into the oculars of the microscope to provide the surgeon with immediate OCT feedback. (C) Custom binocular HUD used to display stereoscopic OCT volumes into the surgical oculars [144]. Volumes rendered from different perspectives were projected into each ocular to provide the surgeon with a stereo presentation of the data in real-time.

Biomedical Optics EXPRESS

5.2 Instrument tracking and robotic-assisted surgery

OCT scans exhibit a trade-off between A-scan sampling density, field of view, and frame-rate. In surgical applications, it is desirable to image the instrument tip and instrument-tissue interactions with the highest sampling density and fastest frame-rate possible, which necessitates small fields of view that may be insufficient to image complete surgical maneuvers. Real-time instrument tracking ameliorates this issue by automatically re-centering the OCT scan on the instrument tip in the presence of motion. El-Haddad *et al.* described a lateral instrument tracking system that used a stereo camera pair to triangulate infrared LEDs mounted to a surgical instrument handle [159]. In later work, they added high-speed reference arm tracking using a Fourier-domain optical delay line [160] to provide a 3D instrument tracking system. The commercial Zeiss RESCAN 700 MIOCT also features reference arm tracking for image stabilization [118].

Additionally, the integration of OCT into surgical instruments (as described in detail in Section 2.3) has facilitated the development of OCT-assisted robotic surgery. In this application, OCT image-based feedback can be used to drive robotic platforms that position surgical instruments with improved precision compared to manual surgery. Yu *et al.* used a forward-imaging OCT probe [105] in conjunction with a master-slave robotic system to evaluate the efficacy of robot-assisted microsurgery with OCT guidance [112,161]. The surgical instrument with integrated OCT was mounted on a custom built seven degree-of-freedom (DoF) Stewart robotic platform, which could articulate the forceps in the X, Y, and Z dimensions, control the roll, pitch, and yaw, and open or close the forceps. The Stewart platform was controlled by a surgeon via a seven DoF haptic device. When simulating retinal surgery, the authors enforced remote center of motion constraints via a software control algorithm that restricted the motion of the forceps once inside the eye to avoid damaging the sclera [112]. The OCT integrated into the instrument permitted constant feedback for improved depth perception during simulated membrane peeling (Fig. 10). In contrast to the master-slave system, other studies explored the utility of OCT-guided cooperative robots, in which the surgeon controlled the robot with their hand instead of a haptic device [107–111]. These robots utilized OCT integrated into the surgical instruments to provide closed loop feedback for applications such as tremor reduction or tool depth locking. Song *et al.* incorporated CP-OCT into two different microsurgical instruments coupled to high speed piezoelectric motors used to drive the axial positioning of the instruments [107,110]. The OCT system did not scan the beam in the transverse plane but was instead used as a single point micrometer-scale axial ranger. Automatic edge detection on the A-scan data allowed the researchers to estimate both hand tremor and the instrument distance to a surface, data which then fed a PID controller that drove the piezoelectric motors for automatic motion compensation. Cheon *et al.* [108] used a more sophisticated real-time surface detection algorithm compatible with layered structures such as retina. This system performed depth locking by using spatially shifted cross-correlation of A-scans to determine the position error of the tip. This position error was then fed into a Kalman filter, which drove the piezoelectric motor via a PD controller.

Biomedical Optics EXPRESS

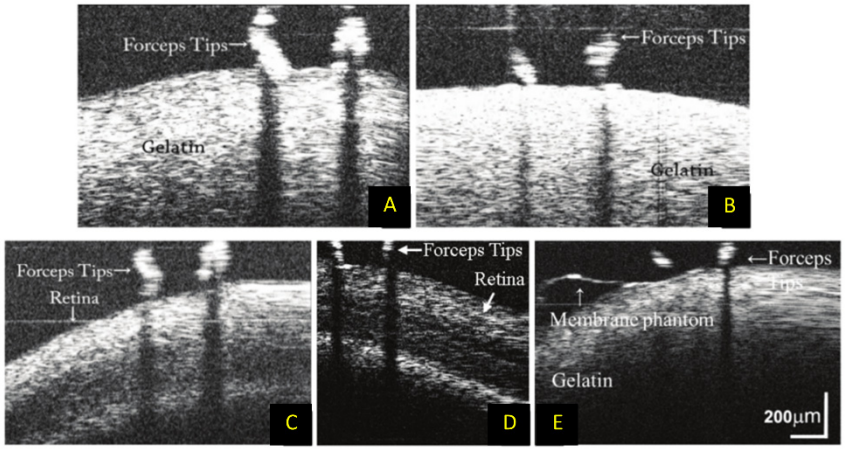

Fig. 10. B-scan imaging of mock surgical manipulations with OCT-integrated surgical forceps and robotic assistance [112]. (A) B-scans of manual and (B) robotic-assisted manipulation of gelatin phantom. (C) B-scans of manual and (D) robotic-assisted manipulation of *ex vivo* goat retina. (E) B-scan imaging during peeling of membrane phantom from gelatin.

5.3 Intraoperative OCT adjuncts

Additional modes of contrast generated from OCT data using various processing algorithms or polarization-sensitive detection have been applied to improve detection of cancerous tissue. An intraoperative HHOCT probe for breast surgery incorporated interferometric synthetic aperture microscopy (ISAM) [162], a computational refocusing algorithm that could yield more uniform lateral resolution along the imaging depth. The resulting OCT images with improved lateral resolution were used to identify tumor margins during human breast surgery [95]. Additionally, variations in collagen orientation and content was also exploited to differentiate cancerous tissue from healthy *ex vivo* breast tissue using polarization-sensitive OCT [163]. Alternatively, Kut *et al.* demonstrated that tissue scattering coefficients estimated from OCT volumes could be used to quantitatively differentiate between cancerous and non-cancerous tissue and help guide brain tumor resections [164]. A color-coded map denoting regions of high scattering and low scattering, corresponding to healthy and normal tissue, respectively, was generated in real-time to provide visual feedback to the surgeon (Fig. 11(a)). The system's algorithm was developed using *ex vivo* human tissues and tested during *in vivo* mouse surgery.

Conventional OCT systems provide only structural information about the sample. Optical coherence tomography angiography (OCTA) is a functional extension of OCT that allows for non-invasive imaging of vasculature without the need for exogenous contrast agents. OCTA has been used to study a wide range of retinal pathologies [165,166] and has been applied in real-time with GPU-accelerated processing [167–169]. Intraoperative OCTA could provide about information about vasculature present in the surgical field to improve surgical decision-making. Intraoperative OCTA using an MIOCT scanner was first reported in 2016 [170], [171]. In particular, in [171] intraoperative OCTA was performed on young children undergoing examination under anesthesia and was demonstrated to provide superior visualization of vasculature compared to FA. Doppler OCT is another functional extension that probes the velocity of moving scatterers within blood vessels to quantify blood flow [172,173]. Doppler OCT processing was incorporated in several HHOCT intraoperative probes to measure blood flow dynamics during animal surgery [100] and during mock surgery using an anastomosis model [91] (Fig. 11(b)).

Biomedical Optics EXPRESS

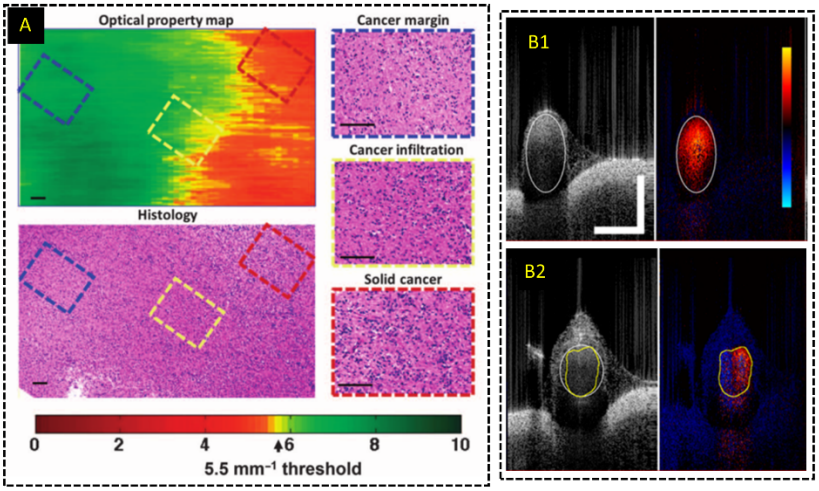

Fig. 11. Functional imaging with intraoperative OCT systems. (A) Optical property map derived from attenuation coefficients calculated from OCT volumes in real-time to differentiate cancerous and non-cancerous tissue [164]. (B) Real-time Doppler processing and imaging for intraoperative HHOCT imaging of anastomoses [91].

6. Intraoperative OCT applications

The translation of medical devices from benchtop to the human operating suite is a nontrivial and often arduous process, requiring compliance with numerous safety requirements set forth by regulatory agencies. These regulations impose technical and engineering constraints that could prevent the use of many research prototypes in a clinical setting. In this section, we primarily focus on research and commercial intraoperative OCT devices that have been successfully translated to the human operating suite and approved for large-scale human clinical studies.

6.1 Human retinal surgery

Dayani *et al.* [80] first demonstrated human retinal intraoperative OCT imaging with a commercial HHOCT device during surgical pauses in 2009. In this study, HHOCT was used to confirm the successful peeling of inner limiting membranes (ILM) and epiretinal membranes (ERM), and it led to the discovery of residual ILM after initial peeling. The residual ILM was subsequently treated during the same surgery, demonstrating the feasibility of HHOCT to alter surgical decision-making. Later studies used a similar commercial HHOCT device to assess macular hole closure in a pediatric case [174] and retinoschisis during treatment of optic pit-related maculopathy [175], and to study the inner retinal surface after peeling of ERMs "with connecting strands" and their correlation to outcomes following ILM peeling [176]. The 2-year PIONEER study [82] conducted in 2014 included 256 eyes, and the authors of the study reported that intraoperative HHOCT imaging impacted the surgeon's decision-making in 63 out of 146 procedures involving ERM peeling. A multitude of other findings stemmed from this study [177,178], including the demonstration of HHOCT for identifying persistent subretinal fluid [179] and HHOCT visualization of peeling-induced retinal alterations resulting from tissue manipulation with intraocular forceps and membrane scrapers [180]. Moreover, Binder *et al.* [116] first demonstrated live 2D MIOCT imaging of human retinal surgery in between surgical steps and before/after surgery using a commercial Cirrus HD-OCT (Carl Zeiss Meditec; Oberkochen, Germany) adapted to the surgical microscope. Imaging of live surgery and instrument-retina interactions with intraoperative MIOCT was demonstrated in three subsequent studies published in quick succession [121], [123,129]. More recently published studies [118,124,181] evaluated the performance of the

Biomedical Optics EXPRESS

commercially available RESCAN 700, specifically. The DISCOVER study was the largest of these to date, comprising 277 eyes, and the researchers reported that MIOCT directly impacted decision-making in 19% of membrane peeling procedures (Fig. 12(a)) [118]. A separate study corroborated these findings and reported that MIOCT altered decision-making in 41.9% of procedures [124]. Lastly, Carrasco-Zevallos *et al.* first reported live 3D (4D) MIOCT of human retinal surgery [122,145,146], and this custom swept-source OCT system was demonstrated to produce B-scans of comparable quality to HHOCT imaging during surgical pauses [182]. In addition, 4D MIOCT provided enhanced volumetric feedback during live surgery, which facilitated recognition of 3D structural alterations after surgical intervention and enabled more complete visualization of surgical maneuvers (Fig. 12(b)) [122]. The live MIOCT volumes were displayed through the microscope oculars during live surgery using a stereoscopic HUD [144]. This system was also recently used to guide the placement of the Argus II retinal prosthesis [183] and to guide choroidal biopsy for choroidal melanoma [184]. Table 1 provides a summary of quantitative results compiled from retinal intraoperative OCT studies performed with HHOCT, live 2D MIOCT, or live 3D MIOCT. Quantitative results from these studies included percentage of surgeries in which of successful intraoperative OCT visualization of the regions of interest was achieved, and percentage of surgeries in which intraoperative OCT directly impacted the surgeon's decision-making.

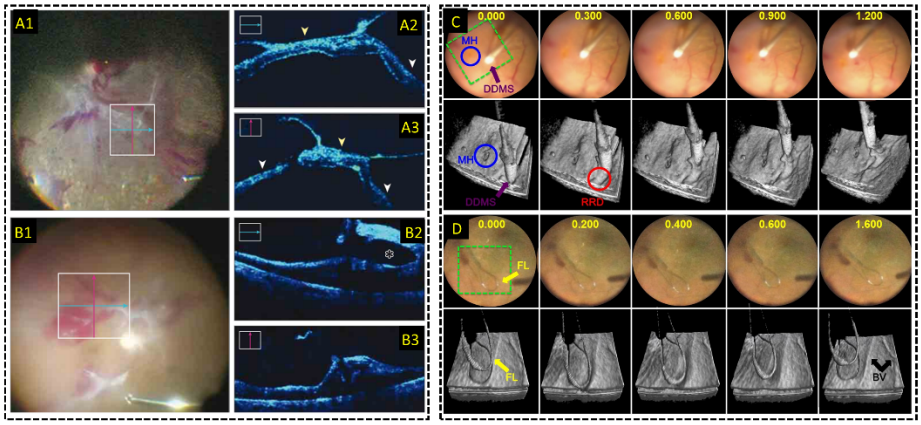

Fig. 12. Live MIOCT imaging during human retinal surgery. (A-B) Live 2D MIOCT imaging with high-resolution orthogonal B-scans using the commercial Zeiss RESCAN 700 [118] during (A) retinal detachment and (B) proliferative diabetic retinopathy procedures. (C-D) Live 3D MIOCT imaging using real-time volumes [122] during retinal brushing with a (C) diamond dusted scraper and a (D) flex loop. High-speed volumetric imaging enhances visualization of subtle 3D tissue deformations.

Biomedical Optics EXPRESS

Table 1. Quantitative results from studies evaluating the efficacy of intraoperative OCT for human retinal surgery. Results are categorized by intraoperative OCT technology and metrics for efficacy, including percentage of surgeries in which successful OCT imaging of the regions of interest was achieved and percentage of surgeries in which OCT altered the surgeon's decision-making. The types of surgical procedures are listed under the percentage values. N/A: not applicable, indicates the researchers did not use this metric in their study. HHOCT: handheld optical coherence tomography. MIOCT: microscope-integrated optical coherence tomography.

	Knecht *et al.* 2010 [185]	**Steven *et al.* 2013** [188]	**Steven *et al.* 2014** [189]	**Ehlers *et al.* 2014** [82]	**Ehlers *et al.* 2015** [118]	**Saad *et al.* 2015** [132]	**Carrasco-Zevallos *et al.* 2016** [122]
Technology	HHOCT	Live 2D MIOCT	Live 2D MIOCT	HHOCT	Live 2D MIOCT	Live 2D MIOCT	Live 3D MIOCT
Successful OCT visualization	6/6 (100%) DSAEK	26/26 (100%) DMEK	6/6 (100%) DALK	518/531 (98%) Anterior segment and retinal procedures	224/227 (99%) Anterior segment and retinal procedures	14/14 (100%) DMEK	15/15 (100%) Multiple types of procedures
Altered decision-making	N/A	N/A	N/A	69/144 (48%) Lamellar keratoplasty	17/51 (33%) Lamellar keratoplasty	N/A	N/A

*Corresponds to percentage of surgeries in which OCT provided *additional* information to the surgeon.

6.2 Human anterior eye surgery

The first use of intraoperative OCT in human anterior eye surgery was demonstrated by Geerling *et al.* in 2005 using a research-grade MIOCT system [113]. Since, HHOCT [82], [185–187] and live 2D MIOCT [118,131,132,188,189] have been implemented to visualize and help guide various anterior eye procedures. Of particular interest were partial corneal transplantation procedures [132,185–189], which require precise depth positioning of the surgical instruments within the corneal tissue. Applications included intraoperative OCT monitoring of separation of Decemet's membrane in deep anterior lamellar keratoplasky (DALK) and confirmation of apposition of the graft to the host tissue [82,118,186,187,189]. Similarly, intraoperative OCT provided improved visualization of the graft orientation and placement beneath the host cornea, and enhanced feedback regarding the apposition of the graft to the host tissue in Decemet's stripping automated endothelial keratoplasty (DSAEK) [82,118,185] and Decemet's membrane endothelial keratoplasty (DMEK) [132,188] (Fig. 13(a)). One study, in particular, reported that a commercial MIOCT system altered surgical decision-making in 48% of lamellar keratoplasty procedures [82]. Live 3D MIOCT was also used during DSAEK to monitor graft placement and graft-host adherence [122] even with a visibly opaque cornea due to significant edema [190] (Fig. 13(b)). The central wavelength of this system was 1040 nm, which enabled deeper visualization into tissue that was opaque in the visible spectrum. This system was also used to visualize needle and suture depth during partial and full thickness muscle passes in strabismus surgery, in which the needle depth cannot be accurately assessed from the superficial *en face* view through the operating microscope [191], and tube shunt positioning in the anterior chamber during glaucoma surgery [192]. Table 2 summarizes quantitative results from various anterior eye intraoperative OCT studies performed with either HHOCT, live 2D MIOCT, or live 3D MIOCT.

OCT-guided femtosecond laser surgery was introduced by Palanker *et al.* in 2010 [73] and has been commercialized by several companies [149]. These surgical platforms, developed primarily for cataract surgery, have demonstrated potential in improving surgical visualization and repeatability [73]. Large-scale clinical trials were conducted to evaluate the

Biomedical Optics EXPRESS

efficacy and safety of commercial femtosecond laser modules with OCT guidance [193], [194] and the researchers reported that OCT aided in detection of the anterior and posterior lens surfaces and iris boundaries [193], and that femtosecond laser cataract surgery with OCT guidance resulted in comparable complication rates to manual surgery [193,194].

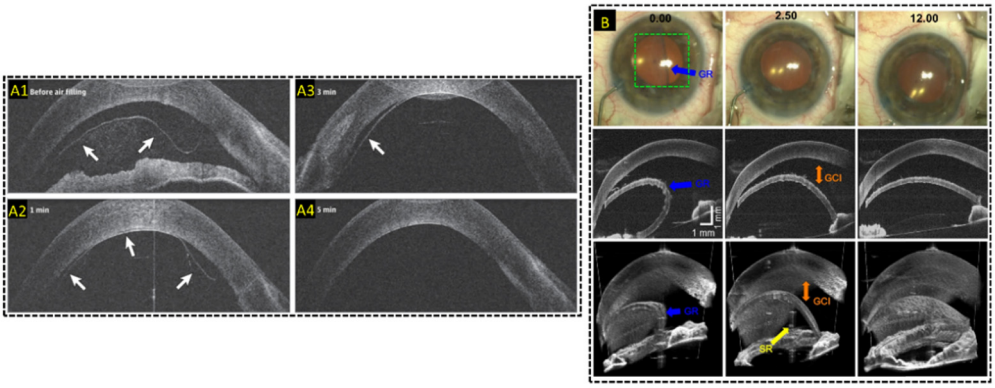

Fig. 13. Live MIOCT imaging of human anterior eye surgery. (A) Live 2D MIOCT imaging with high-resolution B-scans using the commercial Haag-Streit Surgical iOCT [188] during Decemet's membrane endothelial keratoplasty. Real-time direct visualization graft attachment during air filling in B-scans was made possible by MIOCT (B) Live 3D MIOCT imaging using real-time volumes [122] during Decemet's stripping automated endothelial keratoplasty. Graft unfolding, orientation, and apposition was directly visible in the volumes.

Table 2. Quantitative results from studies evaluating the efficacy of intraoperative OCT for human anterior eye surgery. Results are categorized by intraoperative OCT technology and metrics for efficacy, including percentage of surgeries in which successful OCT imaging of the regions of interest was achieved and percentage of surgeries in which OCT altered the surgeon's decision-making. The types of surgical procedures are listed under the percentage values. N/A: not applicable, indicates the researchers did not use this metric in their study. HHOCT: handheld optical coherence tomography. MIOCT: microscope-integrated optical coherence tomography. DSAEK: Descemet's stripping endothelial keratoplasty. DMEK: Descemet membrane endothelial keratoplasty. DALK: Deep anterior lamellar keratoplasty.

	Knecht *et al.* 2010 [185]	**Steven *et al.* 2013** [188]	**Steven *et al.* 2014** [189]	**Ehlers *et al.* 2014** [82]	**Ehlers *et al.* 2015** [118]	**Saad *et al.* 2015** [132]	**Carrasco-Zevallos *et al.* 2016** [122]
Technology	HHOCT	Live 2D MIOCT	Live 2D MIOCT	HHOCT	Live 2D MIOCT	Live 2D MIOCT	Live 3D MIOCT
Successful OCT visualization	6/6 (100%) DSAEK	26/26 (100%) DMEK	6/6 (100%) DALK	518/531 (98%) Anterior segment and retinal procedures	224/227 (99%) Anterior segment and retinal procedures	14/14 (100%) DMEK	15/15 (100%) Multiple types of procedures
Altered decision-making	N/A	N/A	N/A	69/144 (48%) Lamellar keratoplasty	17/51 (33%) Lamellar keratoplasty	N/A	N/A

6.2 Applications in non-ophthalmic human surgeries

The Boppart group at the University of Illinois at Urbana–Champaign leveraged OCT to improve margin analysis in breast cancer surgery. They applied tabletop [195] and handheld SD-OCT [94] systems, in addition to a commercial SS-OCT HHOCT [95], to image pathologic specimens and resection beds intraoperatively for real-time margin analysis. Blinded raters demonstrated a mean sensitivity of 91.7% and specificity of 92.1% for OCT

Biomedical Optics EXPRESS

image-based detection of cancer in *in vivo* resection beds and excised tissue using histopathology as a gold standard [94] (Fig. 14). A similar study, conducted with a commercial HHOCT device, suggested that intraoperative margin analysis in shave margin specimens could reduce reoperation rates at the cost of small increases in resected tissue volume [95]. The Boppart group has also advanced OCT for non-destructive detection of breast cancer metastasis in lymph nodes [196,197]. They proposed using OCT to examine the lymph node cortex *in situ* for metastatic disease, eliminating the need for lymph node dissection and the associated risk of lymphedema. Their recent study in [197] demonstrated a mean sensitivity of 58.8% and specificity of 81.% for identifying reactive/metastatic lymph nodes. The detection sensitivity was complicated by image artifacts and limited depth penetration through tissue overlying the lymph nodes of interest.

OCT probes have also been applied to other resection procedures to improve assessment of the tumor margin. Most of these probes employed ~1300 nm central wavelength to maximize the penetration depth through highly scattering tissue. Compared to histological analysis of excised tissue, which is often time-consuming and expensive, OCT could be used to evaluate the tumor boundaries immediately after surgical excision. Hariri *et al.* applied a research-grade swept-source OCT with 6 µm and 30 µm axial and transverse resolutions, respectively, to differentiate primary lung carcinomas in 82 *ex vivo* tumor samples [198]. The diagnostic accuracy of OCT was 82.6% using histological analysis as the gold standard. Similarly, Hamdoon *et al.* used a commercial OCT probe developed by Michelson Diagnostics to assess oral cancer resection margins [199]. The researchers imaged 112 specimens from 28 patients and determined that OCT could identify positive and negative margins with a diagnostic accuracy of 88%. A different group evaluated the potential of a custom 100 kHz swept-source OCT system for detecting papillary thyroid carcinoma in 170 *ex vivo* tissue samples resected from 17 patients [200]. The sensitivity and specificity of OCT for detecting extrathyroidal extensions was 82.9% and 87%, respectively.

En face full-field optical coherence microscopy (FFOCM) has also been explored for tumor margin assessment in various cancers. In FFOCM, a 2D *en face* image is acquired instantly and the reference arm delay is scanned for tomographic imaging [201]. Compared to traditional OCT, FFOCM uses high NA objectives, yielding improved transverse resolution (1.5 micron in [202]). Using a commercial FFOCM probe developed by AgfaHealthCare in Belgium, Maier *et al.* evaluated 20 freshly excised facial basal cell carcinoma specimens [203]. In this study, FFOCM could identify basal cell carcinoma with a sensitivity and specificity of 74% and 64%, respectively. Additionally, Lopater *et al.* evaluated a commercial FFOCM system (LLTech, SAS) for cancer detection on prostate biopsies [204]. The researchers imaged 119 excised cores from 38 patients, and FFOCM exhibited a cancer detection diagnostic accuracy of 82%. Jain *et al.* also used a FFOCM system from LLTech, SAS, to evaluate fresh tissue sections from tumor and non-neoplastic kidney specimens [202]. The researchers could use FFOCM to subtype 25 tumor specimens with a diagnostic accuracy 80%.

Biomedical Optics EXPRESS

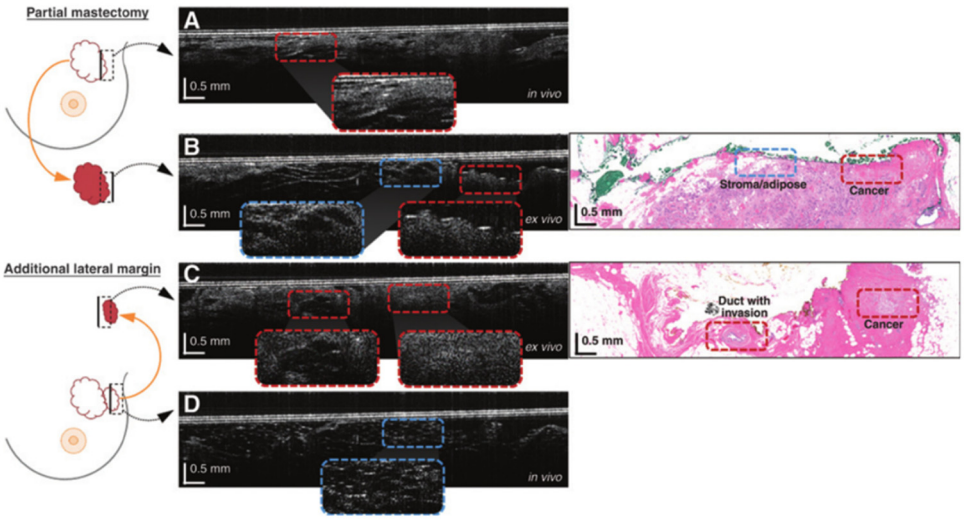

Fig. 14. OCT B-scans acquired with an intraoperative HHOCT probe during breast tumor resection surgery. Diagram on the left denotes tissue areas imaged with OCT B-scan. The blue and red dashed lines in the B-scans correspond to areas of cancerous and noncancerous regions, respectively. (A, C) OCT B-scans of tumor margins acquired *in vivo*. (B, D) OCT B-scans of tumor margins acquired *ex vivo* after resection with corresponding histology [94].

6.3 Live OCT-based surgical training

In addition to human surgical imaging, the potential for MIOCT to improve surgical precision in trainee surgeons has been explored and quantified in *ex vivo* surgical studies [6,122,205,206]. In particular, the impact of MIOCT on surgical residents' performance of ophthalmic maneuvers was studied in [6]. Fourteen ophthalmology residents from the Duke University ophthalmology program, randomized by level of training, were recruited to perform various anterior segment surgical maneuvers on porcine eyes with and without MIOCT guidance. The maneuvers included suture placement at predetermined depths within corneal tissue and creation of triplanar corneal wounds. Active MIOCT guidance helped trainees place sutures at specified depths more accurately. Moreover, when MIOCT was removed, these trainees retained their sense of depth accuracy. This suggested that MIOCT also provided a sustained learning effect for these trainee surgeons. Additionally, another study performed with three retinal surgeons at Duke University explored the ability of MIOCT to improve the depth positioning of instruments during porcine retinal surgery [122,205]. The researchers demonstrated that live MIOCT guidance could improve the accuracy and repeatability of instrument positioning relative to the retinal surface. Subsequent studies explored the viability of MIOCT to quantitatively determine factors that affect successful big-bubble formation during DALK [206,207]. DALK is a technically challenging procedure requiring precise placement of a 27½ gauge needle as deep as possible into the half-millimeter cornea without perforating it. In these studies, novice trainee surgeons using MIOCT were able to successfully place the needle deep into the cornea with perforation rates below those reported in the literature. Further, the depth information provided by MIOCT in these studies also demonstrated that extreme needle depths were not necessary for successful big-bubble formation. Together, these studies of trainees using MIOCT demonstrate the benefits of active MIOCT guidance in improving both accuracy of depth based maneuvers and the potential to reduce depth-related complications in practice.

Biomedical Optics EXPRESS

7. Conclusions

Intraoperative OCT, first introduced in the late 1990's, is currently an area of rapid development driven by academic and industrial research efforts, and it has the capacity to not only improve current surgical efficacy but also to enable the development of surgical techniques dependent on tomographic and volumetric visualization. This review surveyed key technological developments in intraoperative OCT and primarily focused on HHOCT, MIOCT, and OCT-guided laser surgery. Additionally, this review discussed recent clinical studies that demonstrated the utility of intraoperative OCT platforms during human surgery. In the immediate future, we expect further technological improvements and clinical validation to help cement OCT as a vital intraoperative imaging modality with the potential to revolutionize surgical practice.

Funding

This work was supported by National Institutes of Health/National Eye Institute Biomedical Research Partnership grant #R01-EY023039, and a National Science Foundation Graduate Research Fellowship, Ford Foundation Predoctoral Fellowship, and NIH T-32 Training Grant awarded to OMCZ.